Redox Biology 70 (2024) 103081

Contents lists available at ScienceDirect

Redox Biology

journal homepage: www.elsevier.com/locate/redox

FBXL4 protects against HFpEF through Drp1-Mediated regulation of mitochondrial dynamics and the downstream SERCA2a

Miyesaier Abudureyimu [a,b,1], Xuanming Luo [b,c,1], Lingling Jiang [a,b], Xuejuan Jin [b,d,e,f], Cuizhen Pan [b,d,e,f], Wei Yu [g], Junbo Ge [b,d,e,f], Yingmei Zhang [b,d,e,f], Jun Ren [b,d,e,f,*]

[a] Cardiovascular Department, Shanghai Xuhui Central Hospital, Fudan University, Shanghai, 200031, China
[b] National Clinical Research Center for Interventional Medicine, Shanghai, 200032, China
[c] Department of General Surgery, Shanghai Xuhui Central Hospital, Fudan University, Shanghai, 200031, China
[d] Department of Cardiology, Zhongshan Hospital, Fudan University, Shanghai Institute of Cardiovascular Diseases, Shanghai, 200032, China
[e] Key Laboratory of Viral Heart Diseases, National Health Commission, Shanghai, 200032, China
[f] Key Laboratory of Viral Heart Diseases, Chinese Academy of Medical Sciences, Shanghai, 200032, China
[g] Xianning Medical College, Hubei University of Science and Technology, Xianning, 437100, China

ARTICLE INFO

Keywords:
HFpEF
FBXL4
Mitochondrial dynamics
Drp1
Intracellular Ca^{2+}

ABSTRACT

Aims: Heart failure with preserved ejection fraction (HFpEF) is a devastating health issue although limited knowledge is available for its pathogenesis and therapeutics. Given the perceived involvement of mitochondrial dysfunction in HFpEF, this study was designed to examine the role of mitochondrial dynamics in the etiology of HFpEF.

Method and results: Adult mice were placed on a high fat diet plus L-NAME in drinking water ('two-hit' challenge to mimic obesity and hypertension) for 15 consecutive weeks. Mass spectrometry revealed pronounced changes in mitochondrial fission protein Drp1 and E3 ligase FBXL4 in 'two-hit' mouse hearts. Transfection of FBXL4 rescued against HFpEF-compromised diastolic function, cardiac geometry, and mitochondrial integrity without affecting systolic performance, in conjunction with altered mitochondrial dynamics and integrity (hyperactivation of Drp1 and unchecked fission). Mass spectrometry and co-IP analyses unveiled an interaction between FBXL4 and Drp1 to foster ubiquitination and degradation of Drp1. Truncated mutants of FBXL4 (Delta-Fbox) disengaged interaction between FBXL4 and Drp1. Metabolomic and proteomics findings identified deranged fatty acid and glucose metabolism in HFpEF patients and mice. A cellular model was established with concurrent exposure of high glucose and palmitic acid as a 'double-damage' insult to mimic diastolic anomalies in HFpEF. Transfection of FBXL4 mitigated 'double-damage'-induced cardiomyocyte diastolic dysfunction and mitochondrial injury, the effects were abolished and mimicked by Drp1 knock-in and knock-out, respectively. HFpEF downregulated sarco(endo)plasmic reticulum (SR) Ca^{2+} uptake protein SERCA2a while upregulating phospholamban, RYR1, IP3R1, IP3R3 and Na^{+}-Ca^{2+} exchanger with unaltered SR Ca^{2+} load. FBXL4 ablated 'two-hit' or 'double-damage'-induced changes in SERCA2a, phospholamban and mitochondrial injury.

Conclusion: FBXL4 rescued against HFpEF-induced cardiac remodeling, diastolic dysfunction, and mitochondrial injury through reverting hyperactivation of Drp1-mediated mitochondrial fission, underscoring the therapeutic promises of FBXL4 in HFpEF.

1. Introduction

Heart failure with preserved ejection fraction (HFpEF) is the most prevalent form of HF with a normal or near-normal left ventricular ejection fraction [1,2]. Several potential mechanisms have been postulated for the pathogenesis of HFpEF including cardiac remodeling, energetic abnormalities, mitochondrial dysfunction, inflammation, and endothelial injury [1,3,4]. Elevated inflammation and related signaling pathways have also been noted in HFpEF patients based on the PROMIS-HFpEF study [5]. Recent evidence suggested a strong

* Corresponding author. National Clinical Research Center for Interventional Medicine, Shanghai, 200032, China.
E-mail addresses: ren.jun@zs-hospital.sh.cn, zhang.yingmei@zs-hospital.sh.cn (J. Ren).
[1] Equal first authorship.

https://doi.org/10.1016/j.redox.2024.103081
Received 29 January 2024; Received in revised form 8 February 2024; Accepted 8 February 2024
Available online 9 February 2024

association between HFpEF and metabolic dysregulation [6], thus favoring a vital role for inflammation and metabolism in the etiology of HFpEF. Of note, cytokine release and oxidative stress in inflammation and metabolic disarray are well perceived to provoke mitochondrial injury and energy derangement, enroute to the etiology of HFpEF [7].

Mitochondrial homeostasis is governed by synchronized interplay among mitochondrial dynamics, mitochondrial biogenesis, and mitophagy [8–10]. Among which, mitochondrial dynamics functions as an early response element to mitochondrial defect [8,11]. Morphological changes were noted in mitochondrial ultrastructure in a 'two-hit' model of HFpEF, reminiscent of heart tissues acquired from patients with HFpEF [12]. Evident mitochondrial fragmentation, cristae destruction, and vacuolar degeneration were found in HFpEF [7]. Considering the workload of mitochondria to maintain cardiac homeostasis, it is imperative to understand mitochondrial function in HFpEF. Dynamin-related GTPase dynamin-related protein 1 (Drp1), a fission protein, and other fission proteins play an essential role in mitochondrial dynamics [4,13,14]. Mitochondria become elongated in cardiomyocytes with downregulation of Drp1. Mitochondrial translocation of Drp1 is also noted in pathological heart conditions with overtly fragmented mitochondria [15]. Endogenous Drp1 is essential for cardiac hemodynamics, as cardiomyocyte-specific Drp1-knockout mice died prematurely, exhibited defective mitochondrial respiration and buildup of ubiquitinated proteins [16].

Our recent work suggested a role for Skp1-Cullin-F-box (SCF) ubiquitin ligase family in mitochondrial quality control in obese hearts [17]. One important member of SCF ubiquitin family, F-box and leucine-rich repeat 4 (FBXL4), was shown to engage in protein interaction and participate in mitochondrial dynamics, mitochondrial fusion and Ca^{2+} balance through its LRR domain [18]. FBXL4 participates in phosphorylation-directed ubiquitination [19], and plays a crucial role in the maintenance of mtDNA as missense and recessive nonsense mutations of FBXL4 prompt to pathological changes such as lactic acidemia, congenital hypotonia, and mitochondrial encephalomyopathy [20]. Given the ever-rising implication of mitochondrial damage in HFpEF, our current study was designed to evaluate myocardial proteomic alterations of HFpEF with a special focus on mitochondria and FBXL4-governed mitochondrial regulatory components, if any.

2. Materials and methods

2.1. Experimental animals, HFpEF model and plasma file

The experimental procedures used in this work were approved by the Institutional Animal Use and Care Committees of Xuhui Central Hospital and Zhongshan Hospital (Shanghai, China) and were in accordance with the NIH Guideline. In brief, adult male C57BL/6 N mice were randomly assigned to chow or high fat diet (60% of calories from fat) plus L-NAME (0.5 g/L in drinking water) [21]. To evaluate autophagy flux, the lysosomal inhibitor chloroquine (CQ, 20 mg/kg/day, i.p.) was injected intraperitoneally for 7 consecutive days [22]. Mice were anesthetized by a combination of ketamine (80 mg/kg; Pfizer, Berlin, Germany) and xylazine (12 mg/kg; Bayer AG, Leverkusen, Germany). Euthanasia was accomplished by cervical dislocation. Blood glucose levels were measured using a glucometer (Acu-ChekTM). We generated cardiac-specific Drp1 knock-in mice ($Drp1^{CKI}$) by crossing Drp1 and myh6-Cre mice. Heterozygous cardiac-specific Drp1 knockout mice ($Drp1^{hetCKO}$) were generated by crossing Drp1-floxed and myh6-Cre mice. According to the structure of Drp1 gene, exon2-exon7 of Drp1 transcript represents knockout region. Drp1 was knocked out after mating with mice expressing Cre recombinase. Littermates Drp1 flox ($Drp1^{fl/fl}$) mice were used as control group. Genetically engineered mice were purchased from Gem Pharmatech (Nanjing, China) using CRISPR/Cas9-mediated genome engineering [23]. Only male mice (age-matched at 8-10-week-old) were used here to minimize variability.

2.2. Human subjects

A total of 2137 otherwise healthy individuals ≧ 65 years of age were recruited into Shanghai Heart Health Study (SHHS) prior to a baseline survey including general information using self-administered questionnaire, standard 12-lead electrocardiogram (ECG) and chest X-ray. Serum and urine biochemistry were performed. After exclusion of 140 subjects missing serum or urine results, 207 individuals lacking echocardiographic data and 14 subjects with severe valvular dysfunction, 1776 participants were enrolled. Informed consent was obtained from all patients. The study was approved by the institutional human research committee of Zhongshan Hospital Fudan University (2008–10c5), and followed the ethical guidelines stated in the 1975 Declaration of Helsinki.

2.3. Echocardiographic assessment

Mice were anesthetized by isoflurane (1.5–3.0%) prior to measurement of cardiac geometry and function using a 2-D guided M-mode echocardiography (Vevo 2100, Visualsonics, Toronto, ON, Canada). Fractional shortening (FS) was calculated from LV end-diastolic (LVEDD) and LV end-systolic diameters (LVESD) using the equation of (LVEDD - LVESD)/LVEDD. Ejection fraction (EF) and heart rate (HR) were calculated using a Vevo 2100 echocardiography. Peak Doppler blood inflow velocity across mitral valve during early diastole, peak Doppler blood inflow velocity across mitral valve during late diastole, peak tissue Doppler of myocardial relaxation velocity at the mitral valve annulus during early diastole and early filling deceleration time were also recorded. For echocardiogram acquisition in temperature-controlled conditions, isoflurane was reduced to 1.0–1.5% and was adjusted to maintain the heart rate within a range of 450–550 beats per min [24].

2.4. Exercise exhaustion test

After three days of acclimatization to treadmill exercise, an exhaustion test was performed. Mice ran uphill (20°) on the treadmill (Columbus Instruments, Columbus, OH, USA) starting at a warm-up speed of 5 m/min for 4 min before the speed was elevated to 14 m/min for 2 min. Every subsequent 2 min, speed was increased by 2 m/min until mice were exhausted. Exhaustion was defined as inability to return to run within 10 s of direct contact with an electric-stimulus grid. Running time was measured and running distance was calculated [25].

2.5. Blood pressure recordings

Systolic and diastolic blood pressure was measured noninvasively in conscious mice using a CODA tail-cuff device (Kent Scientific, Torrington, CT, USA). Mice were placed in individual holders on a platform, and recordings were performed under steady-state conditions. Blood pressure was recorded for at least three measurements per session [26]. Mice were acclimated for three days prior to measurement to avoid unnecessary interference in blood pressure values.

2.6. Proteomics and enrichment analysis

Protein was extracted from mouse hearts and subjected to NSI source followed by tandem mass tag (TMT)-based mass spectrometry (MS) in Q Exactive™ Plus (Thermo) coupled online to the UPLC. Peptide FDR was adjusted to 1% and all spectra identified with a score <20 was discarded. Proteins meeting the criteria of $|\log2FC| \geqq 1.2$ or $\leqq 0.83$ and p value < 0.05 were identified as differentially changed proteins. These proteins were mapped to the relevant biological annotation and the result of Gene Ontology (GO) and KEGG pathway enrichment analysis was visualized using the 'cluster Profiler' package.

2.7. AAV9 vector production

The recombinant adeno-associated virus (serotype AAV9) was used as vector (Hanbio Biotechnology, Shanghai, China), AAV9-cTNT-GFP (AAV9-NULL) served as the negative control, AAV9-cTNT-FBXL4-3Flag-GFP overexpressed FBXL4 served as the AAV9-cTNT-FBXL4-OE group, and cTNT was employed as the promoter in specific expression in myocardial tissues. Mice were randomly divided into 2 groups, AAV9-cTNT-Null and AAV9-cTNT-FBXL4-OE [27].

2.8. AAV9 FBXL4 injection and transfection in vivo

FBXL4 delivery was achieved in chow and HFpEF mice (following 15 weeks of diet regimen) through tail veins at a dose of 1×10^{12} vg/ml (100 μl per mouse) using an insulin syringe (30-gauge needle) [28]. Eight weeks later, cardiac geometry and function were evaluated using echocardiography while expression of FBXL4 was measured using Western blots and immunohistochemistry.

2.9. Isolation and culture of adult mouse cardiomyocytes (AMCMs)

Following ketamine/xylazine sedation, hearts were removed and perfused with a Krebs-Henseleit bicarbonate (KHB) buffer containing (in mM): 118 NaCl, 4.7 KCl, 1.2 $MgSO_4$, 1.2 KH_2PO_4, 25 $NaHCO_3$, 10 HEPES and 11.1 glucose. Hearts were digested using collagenase D for 20 min prior to removal and mincing of left ventricles. Cardiomyocyte yield at least 80% rod-shaped AMCMs was deemed successful [29]. Cells were transduced with adenoviruses carrying LacZ and FBXL4 (Ad-FBXL4) at the indicated multiplicity of infection (MOI) for 48 h. A cohort of cells for the 'double-damage' cell model was treated with high glucose (HG 12.5 mM) and palmitic acid (PA 0.2 mM) for 12h. For all these treatments, cells cultured in a serum-free medium with dimethyl sulfoxide (DMSO with a final concentration <0.1% without any effect on cell mechanics) were employed as controls [29,30].

2.10. Histological examination

Following anesthesia by a combination of ketamine (80 mg/kg; Pfizer, Berlin, Germany) and xylazine (12 mg/kg; Bayer AG, Leverkusen, Germany), mice were sacrificed and hearts were excised and immediately placed in 10% neutral-buffered formalin at room temperature for 24 h. Cardiomyocyte cross-sectional areas were calculated using a digital microscope (× 400) using the Image J Fiji software (version2.3.0, NIH). Masson trichrome staining was employed to detect fibrosis. Percentage of fibrosis was calculated using the Adobe Photoshop CS3 software (Adobe Systems Inc, San Jose, CA, USA). Fraction of light blue stained area normalized to total area was used as an indicator of myocardial fibrosis. Frozen slices were cut on a cryotome and stained for wheat germ agglutinin (WGA) to measure cross-sectional area of cardiomyocytes [31].

2.11. Detection of reactive oxygen species (ROS)

Myocardial tissue slices were rinsed with 37 °C PBS and incubated with 10 μM DCFH-DA fluorescence probe (Beyotime, China, 1:1000, no serum) for 20 min at 37 °C. Cells were observed using a Leica confocal microscope. ROS fluorescence intensity was evaluated using the ImageJ software [32].

2.12. TUNEL

According to the One Step TUNEL Apoptosis Assay Kit (Beyotime S1086) protocol, frozen heart slices were incubated with TUNEL solution for 1 h prior to fluorescent imaging using the Leica sp8 confocal fluorescence microscope [33].

2.13. Transmission electron microscopy (TEM)

Small cubic pieces $\leq 1\ mm^3$ from left ventricles were fixed with 2.5% glutaraldehyde in 0.1 M sodium phosphate (pH 7.4) overnight at 4 °C. Following post-fixation in 1% OsO_4, samples were dehydrated through graded alcohols and were embedded in Epon Araldite. Ultrathin sections (50 nm) were prepared using an ultramicrotome (Ultracut E, Leica, Wetzlar, Germany), and were stained with uranyl acetate and lead citrate. Specimens were viewed on a Hitachi H-7000 Electron Microscope (Hitachi High Tech America, Inc., Pleasanton, CA, USA) [34].

2.14. Mitochondrial structure analysis

To assess changes in mitochondrial structure, cell was stained with mitochondrial immunofluorescence with Invitrogen MitoTrackerTM Red at 1 mM for10 min at 37 °C. Confocal microscope was used to capture single-cell images assisted by the Image-J software to acquire mitochondrial length.

2.15. Laboratory examination

Blood samples were obtained following a 12-h-overnight fasting and were transferred to central laboratory. Following centrifugation and routine blood test, sera were stored at −28 °C until experimentation.

2.16. Criteria for clinical diagnosis of HFpEF

H2FPEF score was used for discrimination of HFpEF from non-cardiac causes of dyspnea. At a score of ≧6, HFpEF was diagnosed with a probability ≧ 90% with the presence of dyspnea. The 6 variables that constitute the H2FPEF score were (1) a body mass index (BMI) > 30 kg/m^2; (2) use of ≧ 2 antihypertensive medications; (3) the presence of atrial fibrillation; (4) pulmonary hypertension defined as pulmonary artery systolic pressure >35 mmHg; (5) age >60 years; and (6) elevated filling pressures evident from E/e' > 9. The presence of persistent or paroxysmal atrial fibrillation yields 3 points, a BMI >30 kg/m^2 yields 2 points, and all other variables yield 1 point [35]. Exclusion criteria included ejection fraction ≤50% (current or prior), significant valvular heart disease (greater than mild stenosis, greater than moderate regurgitation) and constrictive pericarditis [36].

2.17. Widely targeted metabolomics

Sample quality was monitored by unsupervised PCA (principal component analysis) statistics function prompt within R (www.r-project.org). Significantly regulated metabolites between groups were determined by FDR <0.1 and absolute Log_2FC (fold change) ≧1.2 or ≦0.83. Data were unit variance scaled before unsupervised PCA, calculation of hierarchical cluster analysis and Pearson correlation coefficients [37].

2.18. Cell shortening/relengthening

Mechanical properties of adult mouse cardiomyocytes were assessed using an IonOptix soft-edge system (IonOptix, Milton, MA, USA). Cardiomyocytes were field stimulated at 0.5 Hz. Cell shortening and relengthening were assessed including peak shortening (PS), time-to-PS (TP10, 50, 90), time-to-10%, 50% and 90% relengthening (TR10, 50, 90) and maximal velocity of shortening/relengthening (±dL/dt) [38]. Sarcomere length was assessed including sarcomere length, sarcomere shortening velocity, maximal relaxation velocity, time to peak 90% (TP 90) and time to relengthening 90% (TR 90) [39].

2.19. Measurement of intracellular Ca^{2+} and sarco(endo)plasmic reticulum (SR) Ca^{2+} load

Cardiomyocytes were loaded with 1 μM Fura-2 (Beyotime, S1502) for 20 min, and fluorescence intensity was recorded with a dual-excitation fluorescence photomultiplier system (Ionoptix). Cells were exposed to light emitted by a 75W lamp and passed through either a 360 or a 380 nm filter. Fluorescence emissions were captured between 480 and 520 nm by a photomultiplier tube after first illuminating cells at 360 nm for 0.5 s then at 380 nm for the duration of the recording protocol (333 Hz sampling rate). The 360 nm excitation scan was then repeated at the end of the recording and qualitative changes in intracellular Ca^{2+} concentration were inferred from the ratio of Fura-2 fluorescence intensity (FFI) at two wavelengths (360/380). This "interpolated numerator" method provides better signal-to-noise ratio than the "interleaved" method (rapidly switching between 340 nm and 380 nm wavelengths [29]. Fluorescence decay time (single exponential) was derived as an indicator of intracellular Ca^{2+} clearance [40]. Caffeine-induced release of intracellular Ca^{2+} from SR was used to assess SR Ca^{2+} load capacity. Cardiomyocytes were initially stimulated to contract at 0.5 Hz to ensure steady state. Electrical stimulus was stopped and a caffeine puff (10 mM for 10 s) was applied to proximity of cells through a micropipette to trigger SR Ca^{2+} depletion [41].

2.20. Adenoviral transfection

H9C2 cells were transfected with adenoviruses harboring FBXL4 or Drp1. After adenoviral transfection, cells were subjected to normal or 'double-damage' for 48 h. Cells were transduced with adenoviruses carrying LacZ and FBXL4 (Adv-FBXL4) at the indicated multiplicity of infection (MOI) for 48 h as per the manufacturer's instruction.

2.21. Cell viability assay

Assessment of cell viability was conducted using a commercial CCK8 kit. Cell culture media were introduced with the CCK-8 reagent at a mixed ratio of 1:10 (Beyotime, Shanghai, China).

2.22. Measurement of mitochondrial membrane potential ($\Delta\Psi$)

$\Delta\Psi$ was measured using a ThermoFisher Image-iTTM tetramethylrhodamine, methyl ester (TMRM) kit. Cells were treated with TMRM (50 nM) for 30 min at 37 °C. Samples were visualized and fluorescence intensity was recorded using a fluorescence microscope (Leica sp8, Weztlar, Germany) [32,34].

2.23. Structure-based protein interaction interface analysis between Drp1 and FBXL4

The protein structures of Drp1 were predicted by template-based homology structure modeling tool SWISS-MODEL (www.swissmodel.expasy.org), using Protein Data Bank (PDB) structure 3w6n.1, chain A (covering residues 1 to 364; sequence identity, 93.77%) and FBXL4 structure 6w66.1, chain A (covering residues 278 to 470; sequence identity, 88.85%) as the template. Structures of proteins were submitted to the PRISM tool (http://cosbi.ku.edu.tr/prism) to predict their potential interaction interface. Prediction results were visualized by the PyMol tool (http://pymol.org) [17].

2.24. Immunofluorescence and confocal imaging assay

Immunofluorescence for FBXL4 and Drp1 were performed following the manufacturer's instruction. Briefly, AMCM and H9C2 cell were fixed and permeabilized at room temperature. After blocking for 1 h, samples were incubated with rabbit anti-Drp1 antibody (1:50) and mouse anti-FBXL4 antibody (1:50) overnight at 4 °C. AMCM and H9C2 cells were incubated with anti-rabbit Alexa Fluor 488 (1:800) and anti-mouse Alexa Fluor 546 (1:800 dilution) secondary antibodies for 1 h in the dark. Immunofluorescence was assessed on a laser confocal microscope equipped with a × 630 oil objective (Leica sp8, Weztlar, Germany) [34].

2.25. Co-immunoprecipitation

The co-immunoprecipitation (Co-IP) assay was performed using a TheromFisher Pierce®Co-IP kit follow manufacturer's instructions. One hundred μg of purified anti-FBXL4, anti-Drp1, or anti-flag antibodies were coupled with resin. One mg protein samples were then exposed to the antibody-coupled resin for 2 h. Protein-antibody complexes were eluted in 50 μl elution buffer after mixing and washing. The eluted protein samples were subjected to immunoblotting with corresponding antibodies [42].

2.26. Plasmid constructs and transfection

FBXL4 (NM_172988.4) full-length, Fbox domain deletion (FBXL4-Delta-Fbox), Fbox domain (Fbox), and LRR2 domain deletion (FBXL4-Delta-LRR2) tagged with Flag were cloned in pcDNA3.1-mcherry and purchased from Sai Suofei Genes (Kunshan, China). Drp1 (NM_152816.3) tagged with His was cloned in pcDNA3.1-mcherry and purchased from Sai Suofei Genes (Kunshan, China) [34].

2.27. Ubiquitylation level of Drp1

Immunoprecipitation (IP) with the anti-Drp1 antibody, followed by anti-Ubiquitin (Ub) immunoblotting (IB), was performed in a denaturing RIPA buffer [50 mM Tris-Cl, pH 7.4, 150 mM NaCl, 5 mM EDTA, 1 % (v/v) Triton X-100, 0.5 % sodium pyrophosphate, 0.1 % SDS, and protease inhibitor cocktail (Roche, Basel, Switzerland)]. After tissue or cell lysates were centrifuged at 22,500×*g* at 4 °C for 15 min, supernatants were incubated with anti-Drp1 beads (Shanghai Genomics Inc., Shanghai, China) at 4 °C overnight. Beads were then resuspended and were washed three times with a RIPA buffer (10 min at 4 °C, for each washing), followed by SDS-PAGE and IB analysis with the anti-Drp1/Ub antibodies [42].

2.28. Oxygen consumption rate measurement

OCR was analyzed using an XFe96 extracellular flux analyzer (Seahorse Bioscience). First, Seahorse 96-well plates were attached by polydlysine (PDL) (Sigma-Aldrich) for at least 2 h before AMCMs isolation. Isolated AMCMs were plated on PDL attached dishes at a density of 1×10^5 cells/well and OCR was recorded by sequentially adding the metabolic regulators including oligomycin A (1 μM), FCCP (1 μM), antimycin A (1 μM) and rotenone (1 μM) [32].

2.29. siRNA and transfection

Oligonucleotides for siRNA were made by HanBio. The three pairs of FBXL4 siRNA oligonucleotides were based on the following sequences.

5-GCCCAAAUCUACAAGACUUAA TT-3 (FBXL4 siRNA #1), 5-GCUCUUCUGUUUGUUUGGUUU TT-3 (FBXL4 siRNA #2) and 5-CGUCAGUUUAAACCUUGUAUU TT-3 (FBXL4 siRNA #3). The results were obtained with the second pair, but the third pair was equally effective. H9C2 cells were transfected with siRNA duplexes at a concentration of 75 pM by Lipofectamine 2000 (Invitrogen). At 24 h after the initial treatment, the second siRNA transfection was performed, and cells were grown for 48 h. At 72 h after initial treatment, cells were collected for immunoblotting [43]. A cohort of H9C2 cells were treated with a proteasomal inhibitor MG132 (10 μM, S1748, Beyotime Institute of Biotechnology, Shanghai, China) for 4, 8, and 12 h.

2.30. NAD^+/NADH assay

Murine myocardial lysate contents of NAD^+ and NADH were determined using a NAD^+/NADH Assay Kit (ml092927, mlbio, Shanghai, China) per the manufacturer's manual. The NAD^+/NADH ratio was calculated using standard curves for NAD^+ and NADH [44].

2.31. Aconitase activity

Aconitase activity was determined by monitoring the conversion of isocitrate to *cis*-aconitate, which produces absorbance at a wavelength of 240 nm. The Aconitase Activity Microplate assay kit (ab109712, abcam, Shanghai, China) was employed per the manufacturer's recommended protocol [45].

2.32. Microsome isolation and Ca^{2+}-ATPase activity assay

Microsomes containing ER membrane vesicles were isolated from murine cardiomyocytes using a Beckman ultracentrifuge LE-80K (Brea, CA, USA). ATPase activity of sarco(endo)plasmic reticulum Ca^{2+}-ATPase 2 (SERCA2) was determined through measurement of Ca^{2+} uptake assisted by a Fura-2-based method. Microsomes were incubated in an assay buffer (100 mM KCl, 10 mM HEPES (pH 7.4), 10 mM oxalate, 5 mM $MgCl_2$, 10 μM ruthenium red, and 2 μM Fura-2). The uptake reaction was initiated by addition of 5 mM ATP and 2 μM Ca^{2+}. The fluorescence ratio (excitation at 340 and 380 nm) was recorded at 510 nm emission using a fluorescence microplate reader (BioTek). Rate of Ca^{2+} uptake was derived from the linear slope following addition of Ca^{2+} [46].

2.33. Western blot analysis

Heart tissues were sonicated in a lysis buffer containing 20 mM Tris (pH 7.4), 150 mM NaCl, 1 mM EDTA, 1 mM EGTA, 1% Triton, 0.1% sodium dodecyl sulfate, and a protease inhibitor cocktail. Protein samples were incubated with anti-Drp1, anti-FIS1, anti-MFF, anti-optic atrophy type 1 (OPA1), anti-mitofusin 1 (MFN1), anti-MFN2, anti-FBXL4, anti-ANP, anti-BNP, anti-β-MHC, anti-Caspase3, anti-Caspase9, anti-Caspase12, anti-uncoupling protein 2 (UCP2), anti-Bax, anti-Atg5, anti-LC3BII, anti-p62, anti-*p*-Drp1(Ser^{616}), anti-*p*-Drp1(Ser^{637}), anti-SERCA2a, anti-phospholamban (PLN), anti-ryanodine receptor (RYR1), anti-inositol 1,4,5-trisphosphate receptor 1 (IP3R1), anti-IP3R3, anti-Na^+-Ca^{2+} exchanger (NCX), and anti-translocase of outer mitochondrial membrane 20 (Tom20) antibodies. Horseradish peroxidase-coupled secondary antibodies were employed. All antibodies were obtained from Cell Signaling Technology (Danvers, MA, USA), Santa Cruz Biotech (Santa Cruz, CA, USA) or Abcam (Cambridge, UK). After immunoblotting, films were scanned and detected using a Bio-Rad calibrated densitometer and band intensity was normalized to loading control β-actin or GAPDH [34].

2.34. Statistical analysis

Data were Mean ± SEM. Independent samples *t*-test or Wilcoxon rank sum test for continuous variables and Chi-square test for categorical variables were employed when appropriate to examine differences between HFpEF and non-HFpEF human subjects. Statistical significance was estimated using one-way analysis of variance (ANOVA) followed by Tukey's multiple comparison test, repeated measures ANOVA in R and Bonferroni adjusted test. $^*p < 0.05$, $^{**}p < 0.01$, $^{***}p < 0.001$, and $^{****}p < 0.0001$ were indicated for significance. All statistics analyses were performed using GraphPad Prism 9.0 software (GraphPad, San Diego, CA, USA).

3. Results

3.1. Proteomics analysis and mitochondrial dynamics protein files in HFpEF hearts

To discern biological processes involved in HFpEF, heart tissues were collected from chow and 'two-hit' challenged mice and were subjected to TMT proteomics. Of note, 156 proteins were enriched, 74 proteins were upregulated and 82 proteins were downregulated, and 49% of proteins were localized in cytoplasm and mitochondria. KEGG enrichment analysis revealed that differentially expressed proteins encompassed cGMP-PKG signaling, AMPK signaling and Ca^{2+} signaling proteins within cytoplasm and mitochondria (Fig. 1A–C). Of note, mitochondrion-regulatory proteins, Drp1 and FBXL4 were identified as important candidates among enriched pathways (Fig. 1D). Intriguingly, levels of FBXL4 were downregulated in 'two-hit' hearts (Fig. 1E). Fig. 1F and G also noted upregulated mitochondrial fission proteins including Drp1, FIS1, and MFF as well as downregulated mitochondrial fusion proteins including OPA1, MFN1/2. Supplemental Figs. 1A–B showed altered mitophagy proteins in HFpEF samples including downregulated Pink1 and upregulated Parkin. In addition, autophagy proteins LC3BII and p62 were downregulated and upregulated, respectively, in HFpEF samples, the effects of which were unaffected by CQ injection (Supplemental Figs. 1C–D).

3.2. Effect of FBXL4 transfection on echocardiographic properties in chow and HFpEF mice

To examine possible impact of FBXL4 on HFpEF phenotype, a gain-of-function study was conducted using AAV9 delivery of FBXL4 and vector for 4 weeks (Fig. 2A). Efficacy of FBXL4 overexpression was evaluated using Western blotting (heart, liver, and kidney) and fluorescence imaging (heart) (Fig. 2B–E), revealing a "2-fold" increase in FBXL4 in the heart only. Our result revealed that FBXL4 transfection (but not empty vector) reversed HFpEF-induced rises in septal thickness, LV mass, E wave velocity, A wave velocity, E/A ratio and E/e' ratio as well as decreased e' wave velocity without affecting LV diameters, fractional shortening, and ejection fraction. Transfection of FBXL4 or empty vectors did not elicit any discernible responses in chow mice (Fig. 2F-P, Supplemental Figs. 2A–C). FBXL4 failed to affect 'two-hit' challenge-induced responses in blood pressure, glucose intolerance, plasma insulin and heart rate although it overtly attenuated 'two-hit' challenge-evoked exercise intolerance, cardiac hypertrophy, and pulmonary edema. Empty vector failed to recapitulate FBXL4-offered benefits, nor did it affect body weight, blood pressure, heart rate, insulin levels and insulin sensitivity in chow or HFpEF group (Fig. 2Q-U, Supplemental Figs. 1D–H).

3.3. Effect of FBXL4 overexpression on HFpEF-induced changes in myocardial morphology, oxidative stress, and apoptosis

Our results revealed that the 'two-hit' insult evoked pronounced myocardial interstitial fibrosis, cardiac hypertrophy, oxidative stress, and apoptosis, the effects of which were mitigated by FBXL4 (Fig. 3A–F). Along the same line, 'two-hit' challenge significantly upregulated pro-hypertrophic genes including ANP, BNP, and β-MHC as well as apoptosis markers including cleaved caspase3, cleaved caspase9, and caspase12, the responses were ablated by FBXL4 but not empty vector (Fig. 3G-L). Neither FBXL4 nor empty vector elicited any notable effect on myocardial morphology, oxidative stress, hypertrophic and apoptotic markers in chow-diet group (Fig. 3A-L).

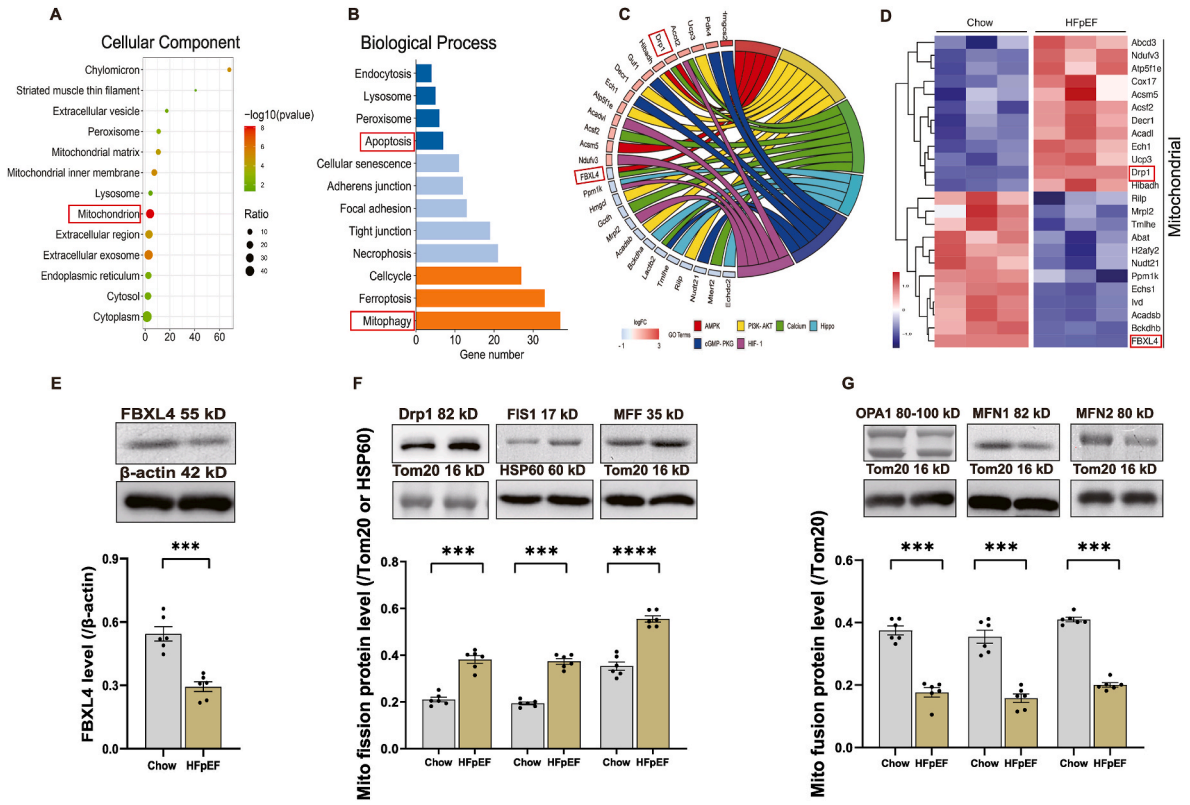

Fig. 1. Adult mice were fed HFD and L-NAME in drinking water for 15 weeks prior to TMT-proteomic analysis of heart tissues. A: Cellular components (CC); B: Biological process (BP); C: Chord diagram displaying the interplay of protein and KEGG pathways; D: Heat map exhibiting up- or down-regulated genes; E: Levels of F-box and leucine-rich repeat protein 4 (FBXL4); F: Levels of mitochondrial fission proteins dynamin-related protein 1 (Drp1), mitochondrial fission protein 1 (FIS1) and mitofusin-1 (MFF); and G: Levels of mitochondrial fusion proteins mitofusin-1 (OPA1), MFN1 and MFN2; Insets: Representative gel bands depicting FBXL4 and mitochondrial fusion/fission proteins using specific antibodies; Mean ± SEM, n = 3 mice for TMT proteomics (panel A–D) or 6 mice per group (panel E–G). Differential proteins were identified using variable important in projection (VIP) > 1.2 in an orthogonal partial least square-discriminant analysis (OPLS-DA) model. Differentially expressed genes were defined as genes with a Benjamini-Hochberg adjusted P value < 0.05. Statistical significance was estimated using one-way ANOVA, ***$p < 0.001$, ****$p < 0.0001$ between indicated groups.

3.4. *Effect of FBXL4 overexpression on HFpEF-induced changes in mitochondrial morphology, dynamics, function as well as intracellular Ca^{2+} transport and autophagy*

Given that HFpEF is associated with mitochondrial fragmentation manifested as smaller and fatter mitochondria [47], we went on to evaluate mitochondrial morphology. Our data noted overtly decreased mitochondrial major axis length and, increased density and circularity in HFpEF mouse hearts, the effect was reconciled by FBXL4 but not empty vector. Mitochondrial number (particularly in the segment of smaller size <0.6 μm) was significantly elevated by HFpEF and reconciled by FBXL4 transfection. Neither FBXL4 nor empty vector elicited notable effect on mitochondrial morphology, dynamics, and function in chow-diet group (Fig. 4A–E). NAD^+/NADH ratio was significantly decreased by HFpEF, the effect of which was reconciled by FBXL4 transfection (Fig. 4F). These data favored a possible contribution of elevated NAD^+ in mitochondria-derived ATP generation. Likewise, aconitase activity was overtly decreased in HFpEF mouse hearts, the effect of which was recovered by FBXL4 transfection (Fig. 4G). Our data also revealed upregulated mitochondrial uncoupling protein UCP2, apoptosis marker Bax and the autophagy adaptor p62 along with suppressed Beclin1, Atg5, and LC3BII in HFpEF hearts, the effect was nullified by FBXL4 but not empty vector (Fig. 4H-M). These results favor the possible involvement of autophagy in FBXL4-offered benefit against HFpEF-induced cardiac anomalies.

Next, we examined mitochondrial dynamics and our result noted upregulated levels of Drp1, Drp1 Ser^{616} phosphorylation (*p*-Drp1 Ser^{616}), *p*-Drp1 Ser^{616}/Drp1 ratio, FIS1 and MFF (fission markers) along with downregulated fusion markers OPA1, MFN1 and MFN2 without changes in Drp1 Ser^{637} phosphorylation in 'two-hit'-challenged hearts. Although FBXL4 did not elicit any effect in chow group, it reversed 'two-hit' insult-induced changes in pan Drp1, Ser^{616} phosphorylation of Drp1, FIS1, and MFF, but not OPA1, MFN1 and MFN2. Empty vector did not elicit any effect on these fission and fusion protein markers (Fig. 5A-L). To understand possible involvement of intracellular Ca^{2+} handling, components responsible for intracellular Ca^{2+} release and re-sequestration were monitored. 'Two-hit' challenge overtly down-regulated intracellular Ca^{2+} regulatory protein SERCA2a while upregulating that of phospholamban, Na^+-Ca^{2+} exchanger (NCX), IP3R1, IP3R3, and RYR1. Transfection of FBXL4 but not LacZ vector rescued 'two-hit' challenge-induced changes in SERCA2a and PLN without affecting other Ca^{2+} regulatory proteins (Fig. 5M-T).

3.5. *Metabolomics analysis in HFpEF of cohort study and in HFpEF mice*

To explore possible underlying pathophysiology mechanisms of HFpEF and the 'two-hit' challenge, metabolomics was conducted in a cohort of HFpEF patients. From 1776 community-based patients after exclusion of HFrEF and patients with valvular diseases, those with HFpEF were identified using the H2FPEF score and clinical symptom to unveil high risk HFpEF cases (2.6%, 46/1776 patients). HFpEF were more likely to be associated with hypertension, atrial fibrillation (AF), coronary artery disease, diabetes mellitus, and dyslipidemia, but less likely obesity. Interestingly, HFpEF patients tended to possess higher levels of total cholesterol, triglyceride, low-density lipoprotein cholesterol and N-terminal pro-B type natriuretic peptide (Supplemental

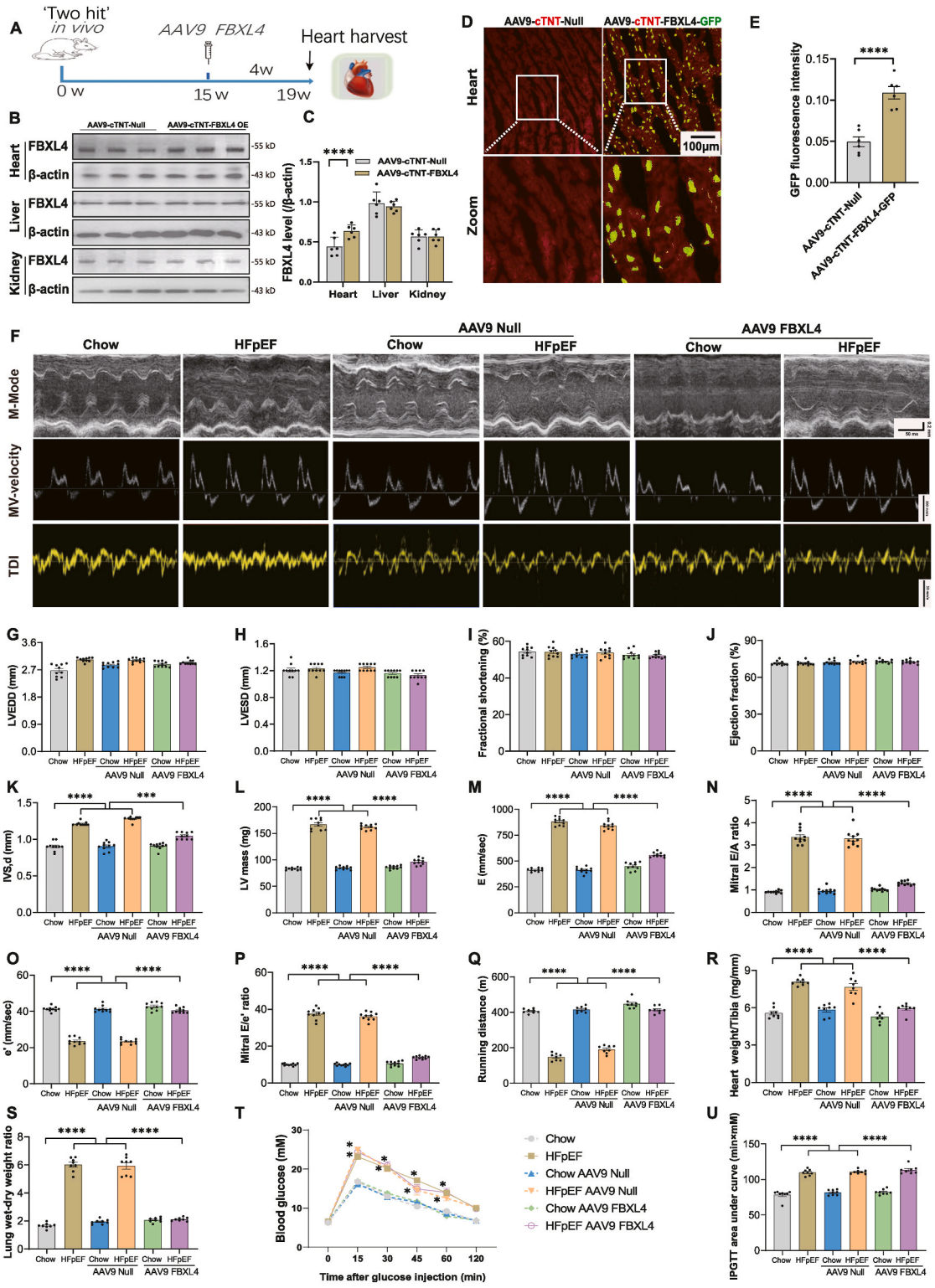

Fig. 2. Verification of FBXL4 levels of AAV viral transfection in mouse hearts, livers, and kidneys, general biometric and echocardiographic properties of chow and 'two-hit' diet-induced HFpEF in mice. A: Illustrative experimental protocol; B: Representative immunoblots of FBXL4 in hearts, livers, and kidneys in AAV9-cTNT-Null and AAV9-cTNT-FBXL4 OE groups; C: Pooled data of FBXL4 in hearts, livers, and kidneys from AAV9-cTNT-Null and AAV9-cTNT-FBXL4 OE groups; D–E: FBXL4 intensity in mouse hearts detected using GFP fluorescence; F: Representative M-mode (upper), pulse-wave Doppler (middle) and tissue Doppler (bottom) images; G: Left ventricular end diastolic diameter (LVEDD); H: Left ventricular end systolic diameter (LVESD); I: Fractional shortening; J: Ejection fraction; K: Interventricular septal thickness in diastole (IVS, d); L: LV mass; M: E wave velocity; N: Mitral E/A ratio; O: e' wave velocity; P: Mitral E/e' ratio; Q: Running distance; R: Heart weight (HW) normalized to tibial length; S: Wet-to-dry lung weight ratio; and T–U: IPGTT curve and area under curve of intraperitoneal glucose tolerance test (IPGTT). Mean ± SEM, n = 6 mice per group for panel B–E, and 8–10 mice per group for others. Statistical significance was estimated using one-way ANOVA followed by a Tukey's post hoc analysis (two-way ANOVA for panel U). *$p < 0.05$, ***$p < 0.001$, ****$p < 0.0001$ between indicated groups.

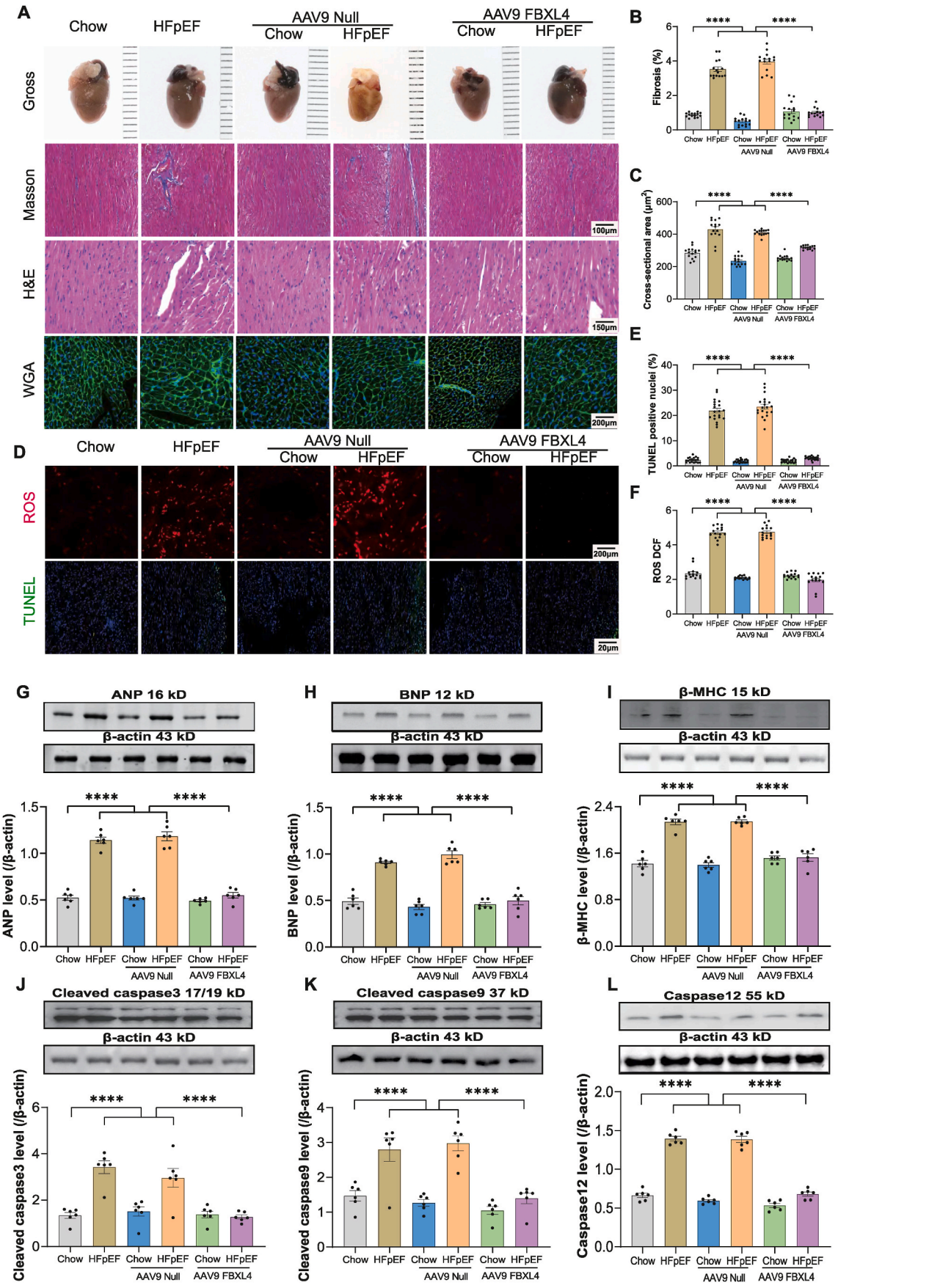

(caption on next page)

Fig. 3. Effect of FBXL4 on HFpEF-induced changes in myocardial morphology, oxidative stress, and apoptosis. A: Representative gross images, Masson trichrome, H&E, and WGA staining; B: Percentage of interstitial fibrosis; C: WGA cross-sectional area; D–F: Representative images and pooled analysis of DCF/TUNEL staining depicting oxidative stress and apoptosis; G: ANP; H: BNP; I: β-MHC; J: Caspase3; K: Caspase9; and L: Caspase12. Insets: Representative immunoblots depicting atrial natriuretic peptide (ANP), brain natriuretic peptide (BNP), β-myosin heavy chain (β-MHC), cleaved caspase 3, cleaved caspase 9, and Caspase12 using specific antibodies. Mean ± SEM, n = 5 mice per group (4 replicates per mouse) (panel A–F) and n = 6 mice per group (panel G–L). Statistical significance was estimated by one-way ANOVA followed by Tukey's multiple comparison test, repeated measures ANOVA in R and Bonferroni adjusted test. ****$p < 0.0001$ between indicated groups.

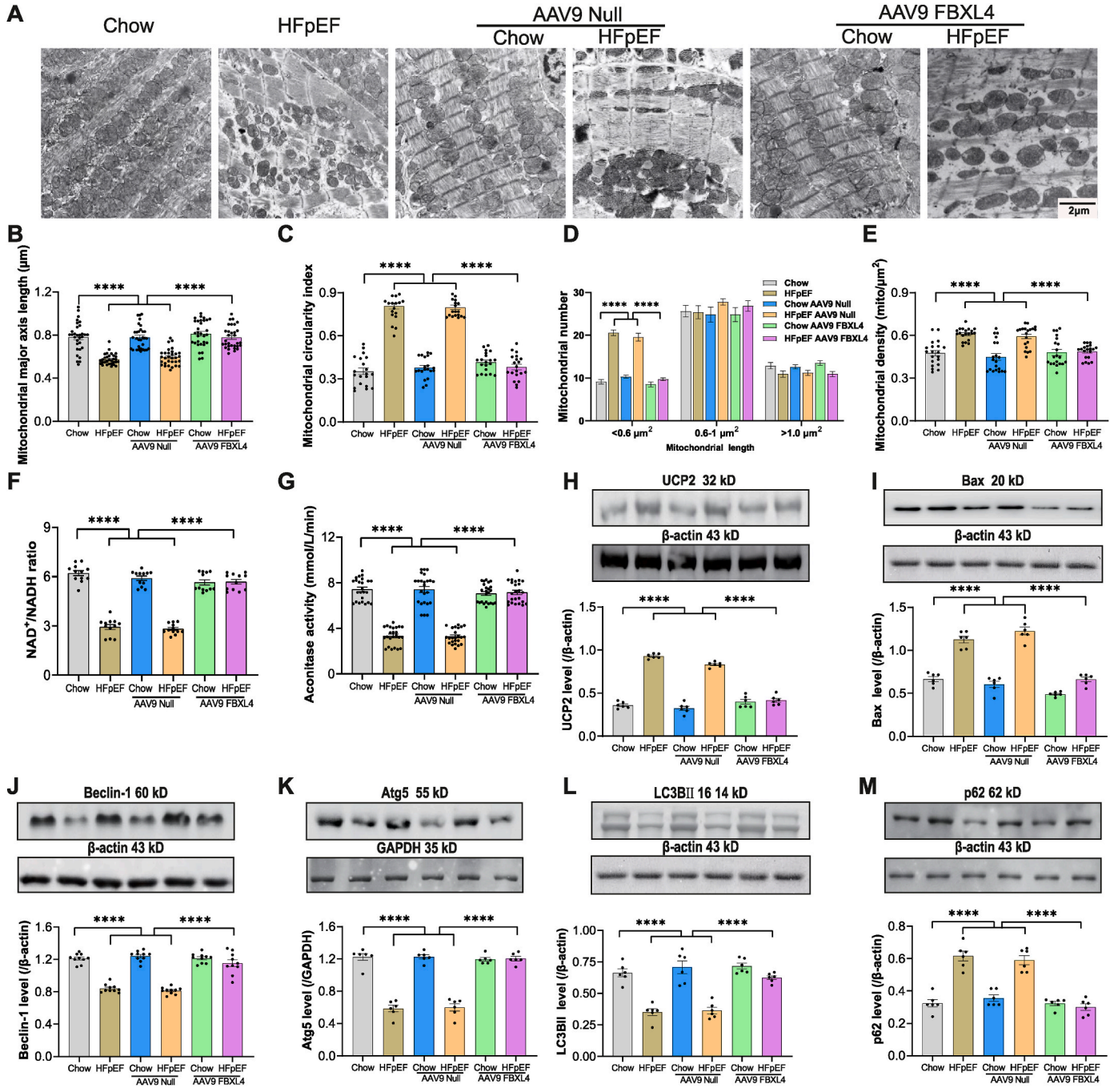

Fig. 4. Effect of FBXL4 on HFpEF-induced changes in mitochondrial ultrastructure, apoptosis, autophagy and mitophagy. A: Representative TEM images; B: Mitochondrial length (major axis); C: Mitochondrial circularity index; D: Mitochondrial distribution by unit size; E: Mitochondrial density; F: NAD^+/NADH ratio; G: Aconitase activity; H: Uncoupling protein 2 (UCP2); I: Bax; J: Beclin-1; K: Atg5; L: LC3BII and M: p62. Insets: Representative immunoblots depicting UCP2, Bax, Beclin-1, Atg5, LC3BII, and p62 using specific antibodies. Mean ± SEM, n = 5 mice per group (4 replicates each mouse, panel A–E), n = 4 mice per group (3 replicates per mouse, panel F), n = 4 mice per group (6 replicates per mouse, panel G), and n = 6 mice per group (H–M). Statistical significance was estimated by one-way ANOVA followed by Tukey's multiple comparison test, repeated measures ANOVA in R and Bonferroni adjusted test. ****$p < 0.0001$ between indicated groups.

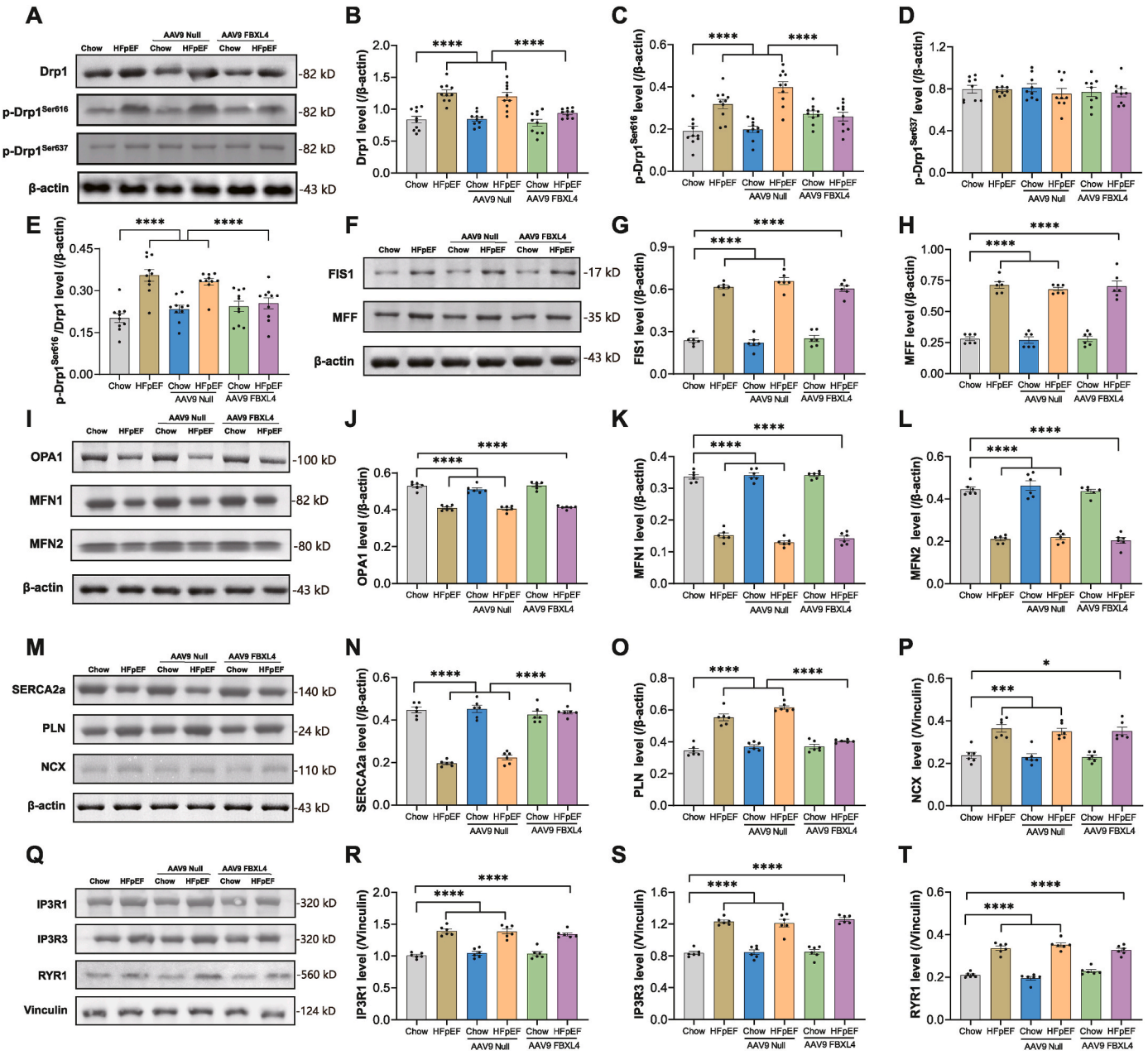

Fig. 5. Effect of FBXL4 on HFpEF-induced changes in mitochondrial dynamics and Ca^{2+} transport. A: Representative immunoblots depicting pan and phosphorylated ($Ser^{616/637}$) Drp1; B: Drp1; C–D: Phosphorylated Drp1 (*p*-Drp1 Ser^{616}, Ser^{637}); E: *p*-Drp1 Ser^{616}-to-Drp1 ratio; F: Representative immunoblots depicting FIS1 and MFF using specific antibodies; G: FIS1; H: MFF; I: Representative immunoblots of OPA1, MFN1 and MFN2 using specific antibodies; J: OPA1; K: MFN1; L: MFN2; M: Representative immunoblots of SERCA2a, PLN and NCX using specific antibodies; N: Sarcoplasmic/endoplasmic reticulum Ca^{2+}-ATPase 2a (SERCA2a); O: Phospholamban (PLN); P: Na^{+}-Ca^{2+} exchanger (NCX); Q: Representative immunoblots of inositol 1,4,5-trisphosphate receptor 1 (IP3R1), IP3R3, and ryanodine receptor 1 (RYR1) using specific antibodies; R: IP3R1; S: IP3R3; and T: RYR1. Mean ± SEM, n = 10 mice per group (panel A–E), n = 6 mice per group (panel F–T). Statistical significance was estimated by one-way ANOVA followed by Tukey's multiple comparison test. $^{*}p < 0.05$, $^{***}p < 0.001$, $^{****}p < 0.0001$ between indicated groups.

Table 1). We performed LC-MS to examine metabolite profiles in human plasma (30 per group including 15 males and 15 females) and HFpEF mouse hearts (6/group). Both human and mouse metabolomic profiles were analyzed using multivariate analysis, while principal component analysis (PCA) and partial least-squares discrimination analysis (PLS-DA) were employed to determine the difference in metabolites. The results indicated a distinct separation in metabolite profiles in HFpEF patients and mice compared with healthy and chow counterparts (Supplemental Figs. 3A–D), indicating altered endogenous substances in HFpEF. Based on PLS-DA analysis, substances with significant differences between two groups were obtained following *t*-test, and endogenous metabolites in plasma and heart tissues were retrieved and matched in HMDB database. These retrieved substances were mainly associated with lipid, amino acid, and carbohydrate metabolism in human plasma and mouse hearts of HFpEF (Fig. 6A and B with male only to avoid possible sex-related issue). Further analysis revealed similar metabolomics pattern in female HFpEF patients or combined patient population (Supplemental Figs. 3E–F). Moreover, proteomics analysis revealed significant association for fatty acid degradation and metabolism with HFpEF in mouse hearts (Fig. 6C). Earlier evidence noted that hearts exposed to hyperglycemic environments with abundant fatty acids in type 2 diabetes mellitus often exhibited LV diastolic dysfunction [1]. To discern a possible role for fatty acid and high glucose in HFpEF, PA (0.2 mM) and HG (12.5 mM) were concurrently exposed to AMCMs

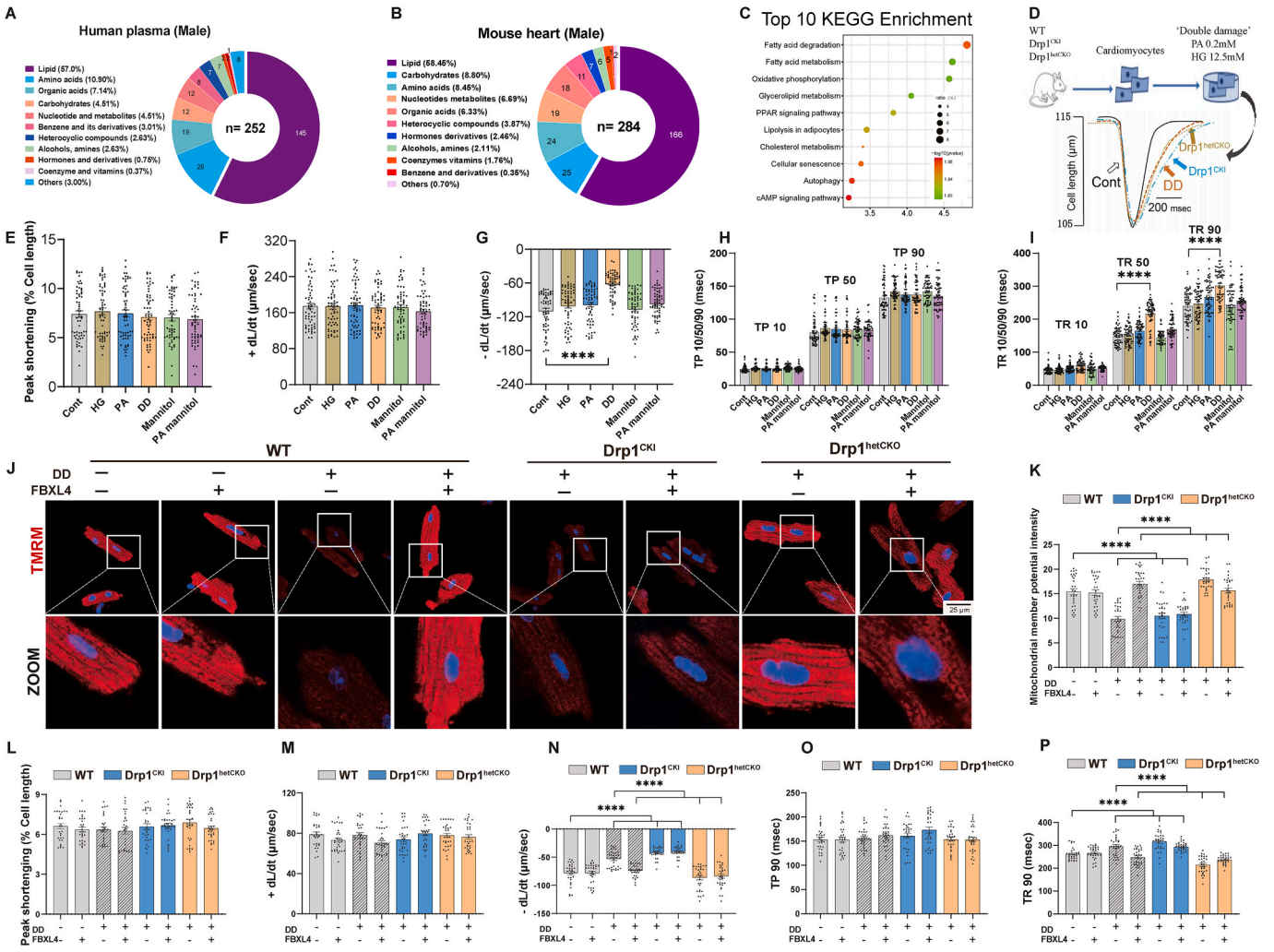

Fig. 6. Metabolomics and proteomics analyses in plasma from HFpEF patients and mouse hearts, as well as establishment of an in vitro HFpEF model for diastolic dysfunction. A: Metabolomics analysis of human plasma (male only) using Mass spectrometry; B: Metabolomics analysis of mouse heart tissues; C: KEGG pathways of top 10 differential proteins from HFpEF mouse hearts using TMT-proteomics; D: Protocol depicting the in vitro 'double-damage' (DD) model established using high glucose (HG, 12.5 mM) and palmitic acid (PA, 0.2 mM) in cardiomyocytes from WT, Drp1^{CKI} and Drp1^{hetCKO} mice; E: Peak shortening (% cell length); F: Maximal velocity of shortening (+dL/dt); G: Maximal velocity of relengthening (-dL/dt); H: Time-to-10%, 50% and 90% shortening (TP10, TP50 and TP90); I: Time-to-10%, 50%, and 90% relengthening (TR10, TR50 and TR90); J: Representative tetramethylrhodamine, methyl ester (TMRM) staining of mitochondrial membrane potential (red color) using confocal microscopy; K: Pooled data of mitochondrial membrane potential using TMRM; L–P: Adult mouse cardiomyocytes from Drp1^{CKI} and Drp1^{hetCKO} mice were transfected with Adv-FBXL4 or vector for 48 h prior to 'double-damage' challenge for another 4 h. L: Peak shortening; M: + dL/dt; N: dL/dt; O: Time-to-90% shortening (TP90); and P: Time-to-90% relengthening (TR90). Mean ± SEM, Independent-samples used *t*-test or Wilcoxon rank sum test for continuous variables and Chi-square test for categorical variables (details provided in Supplemental Table 1); n = 15 subjects (panel A) for metabolomics per group; n = 6 mice (panel B) for metabolomics; n = 3 mice (panel C) for TMT-proteomics, Differential proteins were identified using variable important in projection (VIP) values of >1.2 in an orthogonal partial least square–discriminant analysis (OPLS-DA) model. n = 6 mice per group (10 replicates per heart, panel E–I), and n = 6 mice per group (5 replicates per heart, panel J–P). Statistical significance was estimated using one-way ANOVA followed by the Tukey's multiple comparison test, repeated measures ANOVA in R and Bonferroni adjusted test. ***$p < 0.001$, ****$p < 0.0001$ between indicated groups.

as a 'double-damage' for 12h prior to examination of cardiomyocyte mechanics (Fig. 6D). Our data noted that 'double-damage' challenged cardiomyocytes displayed evident diastolic dysfunction. Systolic function was spared by 'double-damage'. Either PA or HG alone failed to recapitulate 'double-damage'-induced cardiomyocyte mechanical defect (Fig. 6E–I). Cell viability was not notably altered in response to 'double-damage' insult or adenoviral transfection at 12- 24-, 36- and 48-hours (Supplemental Fig. 3G). Overexpression of FBXL4 was validated using Western blot analysis regardless of 'double-damage' insult or not (Supplemental Fig. 3H).

To discern if levels of FBXL4 and Drp1 recapitulate the in vivo 'two-hit' HFpEF model, FBXL4 and Drp1 were also monitored in the 'double damage' cardiomyocyte model. Our data revealed overtly down-regulated FBXL4 along with elevated Drp1 Ser^{616} phosphorylation (Supplemental Fig. 3I). Moreover, endothelial injury is a main feature of heart complications in patients with HFpEF [48]. Levels of eNOS and ET-1 were scrutinized. Our result noted overtly downregulated eNOS level with markedly upregulated vasoconstrictive factor ET-1 in 'double-damage'-challenged mouse artery endothelial cell lines (Supplemental Figs. 3J–K). These findings strongly favor that our in vitro cell model may mimic diastolic dysfunction phenotype reminiscent of HFpEF.

3.6. *Effect of FBXL4 and Drp1 knock-in and knock-out on 'double-damage'-induced cardiomyocyte diastolic dysfunction*

Given the key role of Drp1 in mitochondrial fission, Drp1 knock-in and knockout mice were used to discern the interaction between Drp1

and FBXL4. Meanwhile, using our novel 'double damage' in vitro cardiomyocyte diastolic dysfunction model, possible contributions of FBXL4 and Drp1 in 'double-damage'-evoked diastolic dysfunction were determined using FBXL4 transfection and Drp1 genetic knock-in and knock-out murine models. Our data revealed that FBXL4 effectively alleviated 'double damage'-induced collapse of mitochondrial membrane potentials and diastolic dysfunction in cardiomyocytes. However, FBXL4-offered benefits against 'double-damage'-induced mitochondrial injury and diastolic dysfunction were essentially abolished by homozygous knock-in of Drp1 (Fig. 6J-P). Systolic function manifested by peak shortening was preserved in all groups examined. FBXL4 overexpression did not affect systolic function in $Drp1^{CKI}$ and $Drp1^{hetCKO}$ mice (Fig. 6L-P). Transfection of LacZ vector did not affect 'double-damage'-induced changes in cardiac function and mitochondrial membrane potential in WT and $Drp1^{fl/fl}$ mice (Supplemental Figs. 4A–G).

3.7. Analysis of possible FBXL4-Drp1 interaction and effect of FBXL4 overexpression and Drp1 knock-in, knock-out on mitochondria fragmentation

PRISM technique (http://cosbi.ku.edu.tr/prism) was used to examine potential interaction between FBXL4 and Drp1 and potential interfaces. According to the results from PRISM, Drp1 and FBXL4 may form protein interaction interfaces in Fbox (with CYS-33, GLN-37, LYS-40, ASN-43, LEU-47 as the interaction hotspots) and LRR2 (with ARG-75 as the interaction hotspot) domains on FBXL4 (Fig. 7A and B). To further evaluate if 'two-hit' insult alters Drp1-FBXL4 interaction, co-immunoprecipitation was executed using mouse heart samples following 'two-hit' challenge. Our results failed to discern any difference in Drp1-FBXL4 interaction between the two dietary conditions (Fig. 7C). To explore such interaction, truncated mutants of FBXL4 were constructed with deletion of either Fbox (Delta-Fbox) or LRR2 (Delta-LRR2) domain. Truncated variants of HA-tagged FBXL4 plasmids were transfected with flag-tagged Drp1 plasmid in H9C2 cells. Mutation of Fbox domain disengaged the interaction of FBXL4 with Drp1. However, deletion of LRR2 failed to diminish interaction between Drp1 and FBXL4, suggesting a vital role for Fbox domain of FBXL4 in direct interaction with Drp1 (Fig. 7D). Interaction between FBXL4 and Drp1 was further consolidated using fluorescent colocalization, where mutation of Fbox (but not LRR2) domain disengaged the interaction between FBXL4 with Drp1 (Fig. 7E–G). Likewise, FBXL4 attenuated 'double-damage'-induced mitochondrial fragmentation, the effect of which was cancelled off by Drp1 knock-in (Fig. 7H and I). Transfection of FBXL4 LacZ vector alone did not affect 'double-damage'-induced change in mitochondrial fragmentation in WT and $Drp1^{fl/fl}$ mice (Supplemental Figs. 5A–B).

Ubiquitination and degradation of Drp1 were examined in the presence or absence of autophagy/proteasomal inhibitors or FBXL4 genetic manipulation. Immunoprecipitation data shown in Fig. 7J-M revealed overtly reduced Drp1 ubiquitination in heart tissues from HFpEF mice, the effect of which was reversed by FBXL4 transfection. Application of MG132 removed FBXL4-induced Drp1 degradation, the effect was mimicked by FBXL4 silencing but not scramble siRNA (Fig. 7N-P). In AMCM from HFpEF mice, FBXL4 evoked downregulation of Drp1 in a time-dependent manner, the effect of which was abrogated by MG132 (Fig. 7Q–S).

3.8. Effect of Drp1 knock-in and knock-out on FBXL4-offered protection against mitochondrial damage and diastolic dysfunction in simulated HFpEF, and involvement of ATP dependent-SERCA2a function

To explore possible mechanisms underscoring 'double-damage'-induced cardiomyocyte mechanical changes, intracellular Ca^{2+} handling was scrutinized. Our data depicted that 'double-damage' triggered rises in resting intracellular Ca^{2+} levels (either in 360/380 ratio or calibrated concentration) and prolongation in intracellular Ca^{2+} clearance without affecting electrically-stimulated increase in intracellular Ca^{2+} (ΔFFI, in 360/380 ratio or calibrated concentration). Either HG or PA alone failed to trigger notable intracellular Ca^{2+} changes (Fig. 8A–F). Assessment of sarcomere length displayed shorter sarcomere length, slower relaxation velocity, and prolonged relaxation duration in the absence of changes in sarcomere shortening, shortening duration in cardiomyocytes upon 'double damage' insult (Supplemental Figs. 6A–E), further consolidating diastolic defect observed in cardiomyocyte shortening. Caffeine triggers abrupt release and depletion of Ca^{2+} from SR, the major Ca^{2+} pool available for contractile proteins upon excitation in myocardium [41]. In the presence of 'double-damage' insult, neither baseline FFI nor ΔFFI was altered for caffeine-induced SR Ca^{2+} release (Fig. 8G–J). These findings did not favor a major impact of 'double-damage' insult on SR Ca^{2+} loading capacity, which directly correlates with systolic function.

Given our findings of compromised mitochondrial membrane potentials and downregulated ATP-driven SERCA2a, mitochondrial respiratory oxidation and ATP levels were determined in 'double-damage' challenged cardiomyocytes. Intriguingly, FBXL4-offered beneficial responses were mitigated by SERCA2a inhibitor thapsigargin. Thapsigargin also evoked direct drops in intracellular Ca^{2+} decay in the absence of 'double-damage', the response was unaffected by FBXL4 transfection (Fig. 8K-M). In addition, 'double damage" insult suppressed SERCA2a activity, the effect of which was attenuated by FBXL4 (Supplemental Fig. 6F). Our data shown in Fig. 8N-P noted overtly decreased OCR rate (basal and maximal respiration) in 'double-damage' challenged cardiomyocytes, the effects of which were reconciled by FBXL4. Intriguingly, FBXL4 transfection alleviated 'double-damage'-evoked diastolic dysfunction, the effect of which was abolished by Drp1 knock-in (Fig. 8Q–S). Transfection of FBXL4 LacZ vector alone did not affect 'double-damage'-evoked changes in diastolic dysfunction in WT and $Drp1^{fl/fl}$ mice (Supplemental Figs. 6G–I).

4. Discussion

Our study revealed that FBXL4 rescued against HFpEF-induced cardiac remodeling, pulmonary edema, diastolic dysfunction, exercise intolerance, and mitochondrial injury, with little impact on blood pressure, plasma insulin level and glucose intolerance in HFpEF mice. Our proteomics analysis revealed overt enrichment of Drp1 and the E3 ligase FBXL4 along with mitochondrial fission and cytosolic Ca^{2+} dysregulation in the 'two-hit' HFpEF murine hearts. More importantly, FBXL4 suppressed 'two-hit' HFpEF-induced Drp1 hyperactivation (Ser^{616} phosphorylation) and mitochondrial fragmentation without affecting mitochondrial fusion. Using metabolomics and proteomics approach, unsaturated fatty acids and lipid derangement were unveiled in HFpEF patient plasma and mouse hearts. An in vitro 'double-damage' cell model was established to simulate cardiomyocyte diastolic and mitochondrial defects observed in vivo along with endothelial injury. The 'double-damage' insult did not affect cardiomyocyte SR Ca^{2+} load and systolic (cell and sarcomere shortening) properties, indicating preserved systolic function. Intriguingly, FBXL4 rescued 'double-damage'-induced cardiomyocyte diastolic (cell and sarcomere shortening) and mitochondrial dysfunctions, the effect of which was nullified by SERCA inhibition. This is supported by FBXL4-improved SERCA2a function under 'double-damage' insult. Further scrutiny revealed pronounced energy deficit in 'double-damage'-challenged cardiomyocytes, the effect of which was reconciled by FBXL4. These findings depict a unique cardioprotective role for FBXL4 against HFpEF-evoked pathology through a Drp1/SERCA2a-dependent mechanism.

Ample evidence has revealed pronounced unfavorable changes in myocardial geometry and function in HFpEF including cardiac hypertrophy, interstitial fibrosis, diastolic dysfunction, pulmonary edema, and exercise intolerance [1,49,50]. This is consistent with our observations of cardiac hypertrophy, interstitial fibrosis, preserved fraction shortening and ejection fraction along with diastolic dysfunction

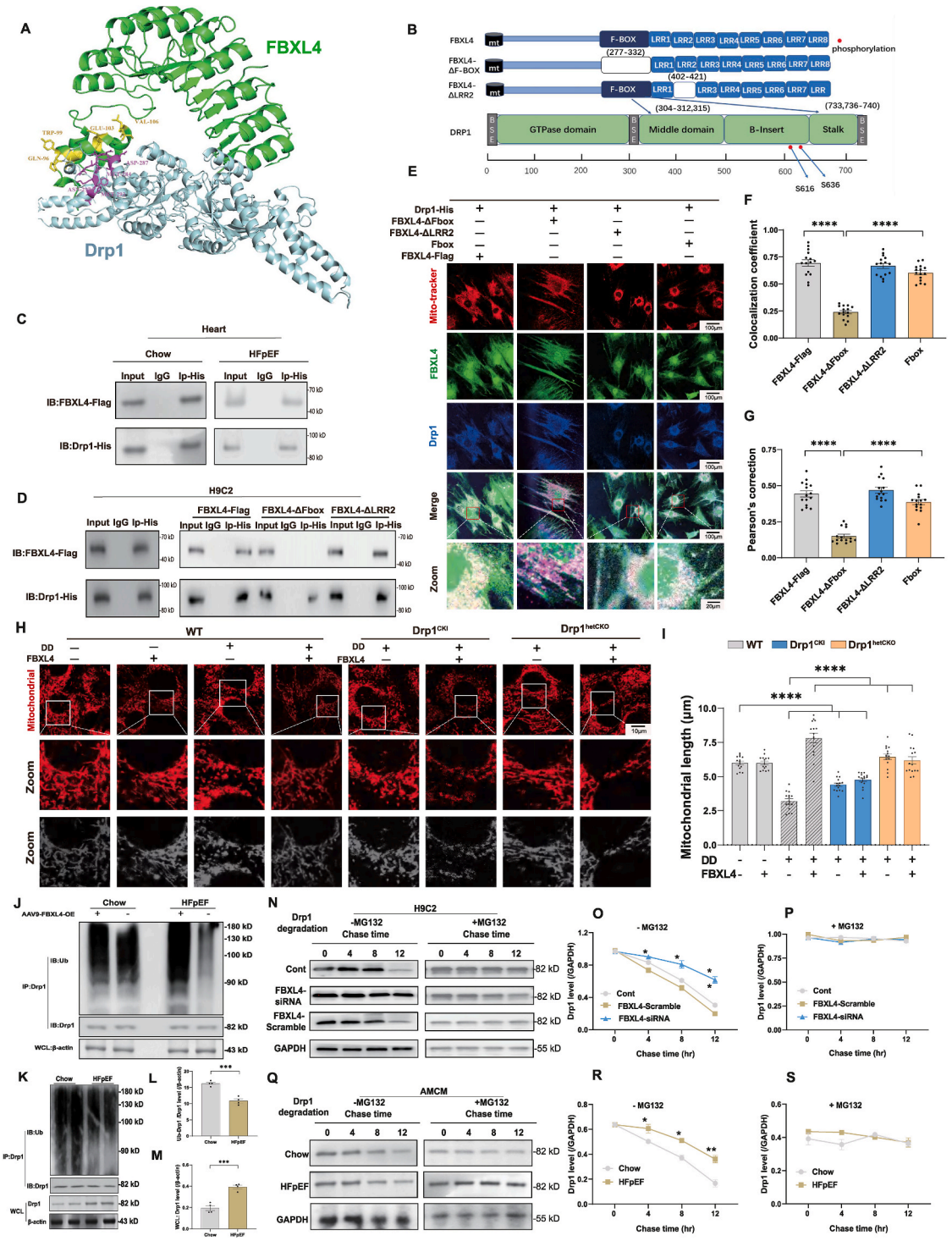

Fig. 7. Detection of Drp1-FBXL4 binding and FBXL4-Drp1 axis in 'double-damage'-evoked mitochondrial fragmentation. A–B: Structure-based interface analysis between Drp1 and FBXL4. A: FBXL4-Drp1 complex structure with interaction hot-spot residues labeled using *PRISM*; B: Domain deletion of FBXL4 for Co-IP experiments, and predicted Drp1 interaction sites on FBXL4. Boxes indicate exons; white bars indicate deleted domains; C: IP analysis of FBXL4 tagged with Flag (FBXL4-Flag) and Drp1 tagged with His (Drp1-His) in AMCM cells from chow and HFpEF; D: IP analysis of FBXL4 domain mutations (FBXL4-Flag, FBXL4-ΔFbox, FBXL4-ΔLRR2) using Drp1-His in H9C2 cell line; E: H9C2 cells were divided into 4 groups (FBXL4-Flag, FBXL4-ΔFbox, FBXL4-ΔLRR2, Fbox) prior to transfection of Drp1 using plasmid DNA, Confocal image exhibiting H9C2 cells transfected with indicated plasmids, stained with MitoTracker (red), anti-FBXL4 (green), and anti-Drp1 (blue) antibodies; F–G: Colocalization and Pearson's correction coefficient; H–I: Assessment of mitochondrial structure using confocal microscopy in adult mouse cardiomyocytes (AMCM) transfected with Adv-FBXL4 for 48 h prior to DD challenge for 12 h; H: Representative mitochondrial immunofluorescence using Mito Tracker (red); and I: Quantification of mitochondrial length of $Drp1^{CKI}$ and $Drp1^{hetCKO}$ groups. J–M: Ubiquitylation level of Drp1 in heart tissues from chow and HFpEF with or without FBXL4 overexpression; N–P: Drp1 level in H9C2 cells transfected with FBXL4-siRNA or FBXL4-scramble, treated with or without MG132 for 4, 8, and 12 h; Q–S: Whole cell level of Drp1 treated with or without MG132 for 4, 8, and 12 h in AMCM cells from chow and HFpEF; Mean ± SEM, n = 3 mice per group (5 replicates per heart, panel E–I), or 3 replicates from 1 sample per group (panel J–M), or 2 replicates from 3 sample per group (panel N–S). Statistical significance was estimated by one-way ANOVA followed by the Tukey's multiple comparison test or repeated measures ANOVA in R and Bonferroni adjusted test. $^{*}p < 0.05$, $^{***}p < 0.001$, $^{****}p < 0.0001$ between indicated groups.

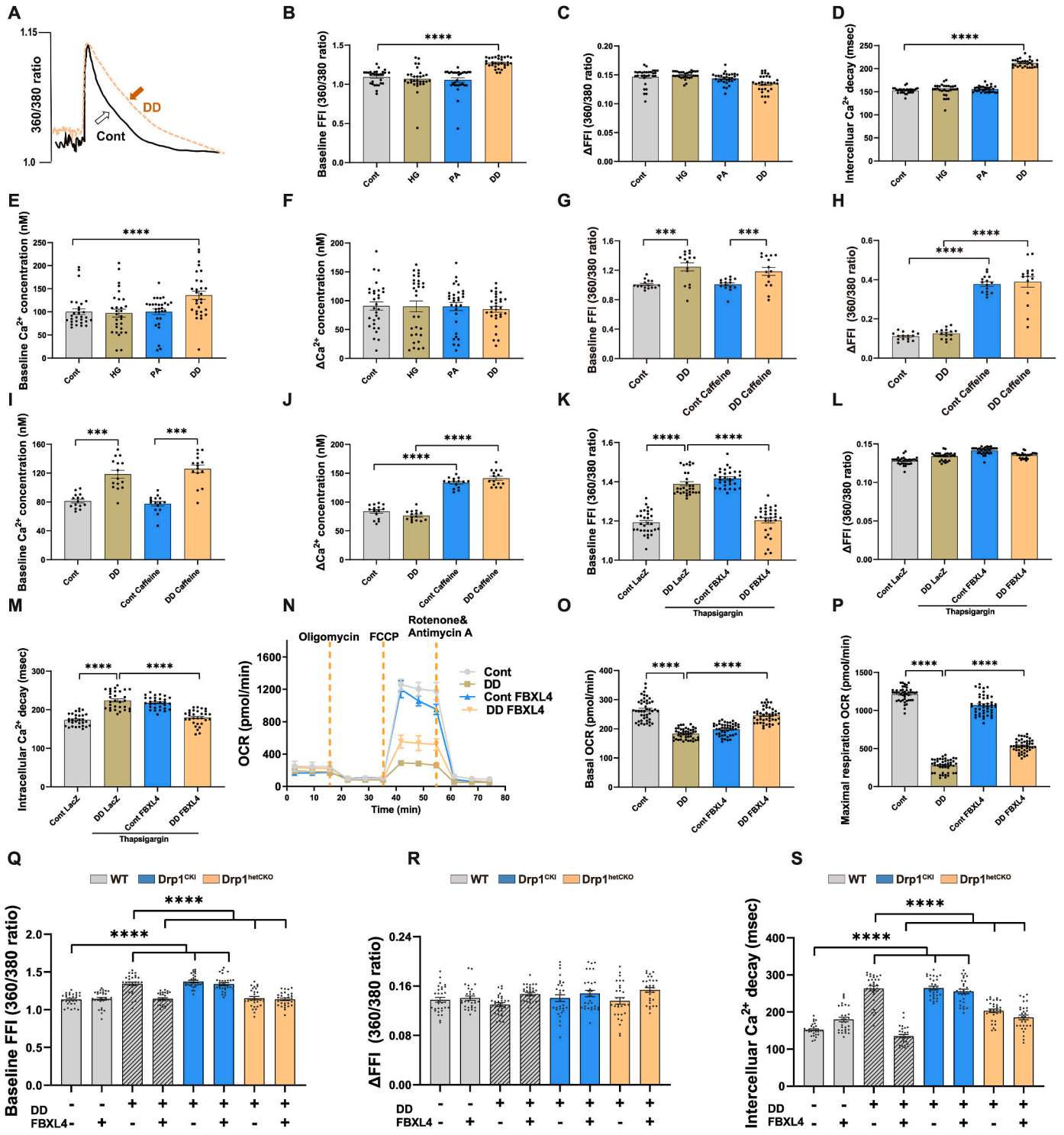

Fig. 8. Role of ATP-dependent SERCA2a/PLN and Drp1 in FBXL4-offered benefits in 'double-damage' cell model. A–F: Experiments depicting intracellular Ca^{2+} transient properties in control and 'double damage' (DD) mouse cardiomyocytes; G–J: Caffeine-induced changes in baseline fura-2 fluorescence intensity (FFI), ΔFFI and intracellular Ca^{2+} decay rate; K–M: Impact of SERCA inhibition using thapsigargin (Tg) on FBXL4-offered benefit against DD-induced intracellular Ca^{2+} mishandling including baseline Fura-2 fluorescent intensity; N–P: Effect of FBXL4 on DD-induced myocardial energy deficit using OCR curve (panel N), basal OCR and maximal respiration (panel O–P); and Q–S: Effect of Drp1 knock-in or knock-out in FBXL4-offered intracellular Ca^{2+} responses under DD challenge. Cardiomyocytes from WT, $Drp1^{CKI}$ and $Drp1^{hetCKO}$ mice were challenged with DD regimen for 12 h in the absence or presence of FBXL4 overexpression; Mean ± SEM, n = 6 mice per group (5 replicates per heart, panel B–F, K–S), n = 5 mice per group (3 replicates per heart, panel G–J). Statistical significance was estimated using one-way ANOVA followed by the Tukey's multiple comparison test or repeated measures ANOVA in R and Bonferroni adjusted test. ***$p < 0.001$, ****$p < 0.0001$ between indicated groups.

(increased E wave, E/A ratio and E/e' ratio as well as dropped e' wave, –dL/dt and prolonged relengthening duration) following 'two-hit' challenge. In our hands, a tight association was evident between mitochondrial dynamics and mitochondrial injury under the 'two-hit' challenge. KEGG enrichment identified FBXL4 in 'two-hit' insult-induced diastolic dysfunction along with Drp1. Western blot analysis noted upregulated mitochondrial fission proteins, downregulated mitochondrial fusion proteins and FBXL4 in 'two-hit' hearts. Mutation of FBXL4 was demonstrated to evoke fragmentation of mitochondrial network, suggesting a role of FBXL4 in mitochondrial dynamics [51]. Likewise, absence of FBXL4 leads to aberrant changes in mitochondrial proteins and mitochondrial function through degradation of mitochondria [19]. Examination of human genes associated with encephalopathy also revealed an etiological role for mutant FBXL4 in mitochondrial swelling and mitochondrial respiratory dysfunction [52,53]. Mitochondrial phenotypic changes included mitochondrial fragmentation, decreased basal and maximal respiration, impaired survival under obligate aerobic respiration, and lost mitochondrial inner membrane potential under FBXL4 deficiency [54]. Our data unveiled evident oxidative stress, apoptosis (Bax, cleaved caspase-3 and -9), deranged autophagy (LC3B, p62) and mitophagy (Pink1 and Parkin) along with mitochondrial injuries following 'two-hit' insult, denoting a role for mitochondrial dynamics in HFpEF injury. These findings coincide with the enrichment of "apoptosis" and "mitophagy" processes from TMT proteomics in HFpEF hearts. Intriguingly, FBXL4 attenuated 'two-hit' insult-induced apoptosis, deranged autophagy, overactivation of Drp1 and mitochondrial fission.

Perhaps the most innovative finding from our work is that Drp1 interacts with FBXL4 while forced expression of Drp1 abolished FBXL4-offered protection against HFpEF. PRISM and co-IP analyses indicated a direct interaction between FBXL4 and Drp1 through Fbox domain (CYS-33, GLN-37, LYS-40, ASN-43, LEU-47 as the interaction hotspots) on FBXL4. Drp1 is a crucial 'adapter' in mitochondrial fission and maintains mitochondrial integrity [55]. Mitochondrial fission is turned on in response to Drp1 relocation onto outer mitochondrial membrane (OMM) and its subsequent activation (phosphorylation). Nonetheless, a paradoxical role was reported for Drp1 with regards to cardiac homeostasis [55]. Inhibition of Drp1 was found to mitigate mitochondrial injury, unveiling a crucial role for Drp1 in the governance of mitochondrial homeostasis. These notions are consistent with our findings of mitochondrial dysfunction and contractile defects with hyperactivation of Drp1 in HFpEF model. Nonetheless, an obligatory role for endogenous Drp1 was suggested in preservation of cardiac homeostasis in stress conditions [23]. In Drp1 deficient cardiomyocytes, mitochondria displayed higher connectivity, buildup of ubiquitinated proteins, and decreased respiration. Disruption of Drp1 triggers mitochondrial elongation, suppresses mitophagy, and evokes mitochondrial injury, thus promoting cardiac dysfunction [56]. In our hands, we noted hyperactivation of Drp1 along with Fis1 (a Drp1 receptor) [57]and MFF, in HFpEF model. Fis1 assemblies fission apparatus resulting in mitochondrial membrane constrictions and division [57]. MFF then fosters mitochondrial recruitment of Drp1 and mitochondrial fission. Thus, upregulation of Drp1, MFF, Fis1 collectively favors a coordinated mitochondrial fission event centered around Drp1 [58].

Our data noted Drp1 hyperactivation in association with more pronounced mitochondrial impairment, mitochondrial energy defect (OCR) and Ca^{2+} overload following the 'two-hit' insult. Drp1 hyperactivation-induced mitochondrial fragmentation (under 'two-hit' or 'double-damage') then disrupts mitochondrial ultrastructure and integrity, resulting in collapsed mitochondrial membrane potential and loss in mitochondrial energy (ATP levels and OCR respiration). It is noteworthy that mitochondrial injury is associated with diastolic but not systolic dysfunction (evidenced by preserved systolic parameters and SR Ca^{2+} loading capacity) in our experimental settings. Earlier evidence has indicated a close tie between mitochondrial OXPHOS function and contractile capacity in the heart although mild to moderate mitochondrial injury may impose local or temporal accumulations of ADP and impair SERCA2a function, enroute to elevated cytosolic Ca^{2+} level, cardiac stiffness, and diastolic anomalies in HFpEF models [59]. Higher cytosolic Ca^{2+} (also seen in our current study) may evoke ROS accumulation, oxidation of CaMKII to favor relaxation defect through SERCA2a loss and cell death in cardiomyocytes [60]. Thus, it is possible that development of moderate mitochondrial injury may be responsible for diastolic but not systolic defect as seen in our 'two-hit' model. Nonetheless, timely diagnosis of mitochondrial injury and HFpEF is rather challenging given the difficulty of non-invasive characterization of symptoms of reduced heart pump capacity to deliver blood at normal filling pressures during diastole [3,35,61]. Patients often exhibit hemodynamic abnormalities only under stress (e.g., exercise) condition. Hinted by metabolomics findings from human and murine HFpEF subjects, we established a novel 'double-damage' model using concurrent exposure of palmitate and high glucose, two likely triggers for lipotoxic challenge in metabolic derangement [62]. Using this model, we were able to mimic the in vivo 'two-hit' HFpEF-evoked cardiomyocyte diastolic dysfunction, SERCA2a defect and mitochondrial anomalies, the effect of which was alleviated by FBXL4. Data from CCK8 assay did not favor a major role for altered cell viability in 'double damage'- or FBXL4-induced changes in cardiomyocyte function. Intriguingly, FBXL4-offered beneficial responses were abrogated by Drp1 knock-in or SERCA2a inhibition. Likewise, FBXL4-offered benefit against 'two-hit'-induced mitochondrial energy deficit (ATP level and mitochondrial respiration) and intracellular Ca^{2+} derangement was nullified by Drp1 knock-in, supporting a downstream role for ATP-dependent SERCA in FBXL4/Drp1 axis under HFpEF.

Several scenarios may be considered for FBXL4-Drp1 axis in 'two-hit'-evoked myocardial anomalies. FBXL4 comprises canonical FBXL functional domains [63]. Importantly, FBXL4 contains a mitochondrial localization sensor, allowing its colocalization with mitochondrial proteins [53]. In our hands, FBXL4 interacted with Drp1 through F-box domain on FBXL4 to speed up Drp1 ubiquitination/degradation to keep mitochondrial fission in check. We found that FBXL4 may bind Drp1 to promote its ubiquitination/degradation. Our data indicated that FBXL4-induced Drp1 degradation was overtly increased by FBXL4 overexpression, favoring a ubiquitin-proteasomal dependent mechanism in Drp1 degradation in the face of 'two hit' insult. With reduced availability of mitochondrial energy, diastolic function and SERCA2a level/function were compromised, leading to poor intracellular Ca^{2+} clearance and cytosolic Ca^{2+} overload. Loss of FBXL4 in HFpEF would dampen FBXL4 interaction and degradation of Drp1, trigger mitochondrial fragmentation and injury, ultimately compromising mitochondrial energy and SERCA2a function. Involvement of SERCA2a, a driving force for intracellular Ca^{2+} re-sequestration into SR and diastolic function, in FBXL4-offered cardioprotection against HFpEF pathology received further supports from the observation that SERCA2a inhibitor thapsigargin nullified FBXL4-induced cardioprotective responses.

Our results revealed elevated resting cytosolic Ca^{2+} and unchanged caffeine-evoked SR Ca^{2+} load in 'double-damage' cell model, indicating preserved systolic function along with diastolic defect. Earlier findings noted mixed findings with regards to the correlation between SERCA defect and contractile function. In particular, reduced SERCA2a levels (in some cases, along with poor Na^{+}/Ca^{2+} exchange function), were found to be associated with systolic dysfunction, possibly due to inadequate SR reuptake, resulting in elevated cytosolic Ca^{2+} levels and low SR Ca^{2+} capacity available for the next systole mainly driven by ryanodine receptors, myofilament Ca^{2+} sensitivity and myofilament cross-bridge sliding [64,65]. Loss in SERCA function likely brings on compensatory intracellular Ca^{2+} regulatory components such as mitochondrial Ca^{2+} uptake and sarcolemma Na^{+}-Ca^{2+} exchange, to replenish SR with sufficient Ca^{2+} load (although at a much slower rate) to preserve intracellular Ca^{2+} release and systolic function. This is supported by preserved SR Ca^{2+} load and systolic function in the face of overtly reduced SERCA2a levels in cardiac pathological conditions such

as diabetes [66,67], as seen in our present study.

4.1. Experimental limitations

Certain experimental limitations exist for our study. First, species differences (in vivo, in vitro and cell lines) employed in our study present an obstacle to limit our understanding of authentic pathogenesis and targeted therapies for HFpEF. The HFpEF cohort is accompanied with more cardiovascular complications, including hypertension, diabetes, and hyperlipidemia, clearly distinct from our 'two-hit' murine model. The apparent HFpEF rate of 2.6% create a dramatic difference in sample size (thus possibly affecting statistical outcome) between HFpEF versus non-HFpEF groups. HFpEF prevalence was reported to be 3.8–7.4% in other cohort studies, similar to our study [68,69]. Due to apparent ethical issue, we cannot collect heart tissues from HFpEF patients to verify levels of FBXL4 and Drp1 or metabolomic analysis. Next, only male mice were used in our study, creating a possible sex-related issue. Also, plasma omics was not comparted between human and rodent, creating a potential organ-dependent bias. Although our metabolomics results did not reveal any notable sex difference in human HFpEF patients, larger patient population at different ages should be examined. Based on CHARM-preserved, I-PRESERVE, and TOPCAT study, younger patients with HFpEF were more often obese black or Asian men with a lower comorbidity burden. However, older patients with HFpEF were more often white women who exhibited higher comorbidity burden compared with younger patients [70]. Since our current study did not directly involve an "aging" aspect, possible sex issue may not be as a major impact as those in older mice. Third, dampened autophagy (likely due to lysosomal defect as shown by autophagy flux experiment) was noted in our 'two-hit' HFpEF model, which was greatly reversed by FBXL4. Given the close association between mitochondrial integrity and autophagy [8,71], improved autophagy (and autophagy flux) in response to FBXL4 may be resulted from improved mitochondrial function although further study is warranted to discern the role of autophagy in HFpEF. Fourth, the 'two-hit' model represents nitrosative stress with concurrent obesity and hypertension [21]. Cardiac dysfunction in high fat diet-induced obesity is manifested as decline of both systolic and diastolic function [17,62], which is phenotypically different from HFpEF. KEGG analysis from obese hearts enriched mitophagy pathway rather than mitochondrial dynamics among top hits [17]. In this context, mitochondrial dynamics may play a more dominant role in HFpEF although further study is warranted for mitophagy in HFpEF. Last but not the least, our in vitro 'double-damage' model mimicked diastolic, SERCA2a and mitochondrial dysfunctions in HFpEF. It should be mentioned that this 'double-damage' in vitro model may not recapitulate authentic pathophysiological milieu of HFpEF cardiomyocytes in vivo. A more thorough screening of various metabolites in HFpEF should uncover the proof-of-concept applicability of metabolomics for the treatment in HFpEF.

In summary, we provided evidence that FBXL4 rescued against HFpEF-induced cardiac remodeling, diastolic and intracellular Ca^{2+} dysregulation through Drp1/SERCA2a-dependent regulation of mitochondrial integrity and cytosolic Ca^{2+}. FBXL4 likely bound Drp1 to evoke Drp1 degradation in a proteasomal-dependent manner, thus reverting hyperactivation of Drp1-mediated mitochondrial fission (Fig. 9). These findings favored the notion that FBXL4 and Drp1 may

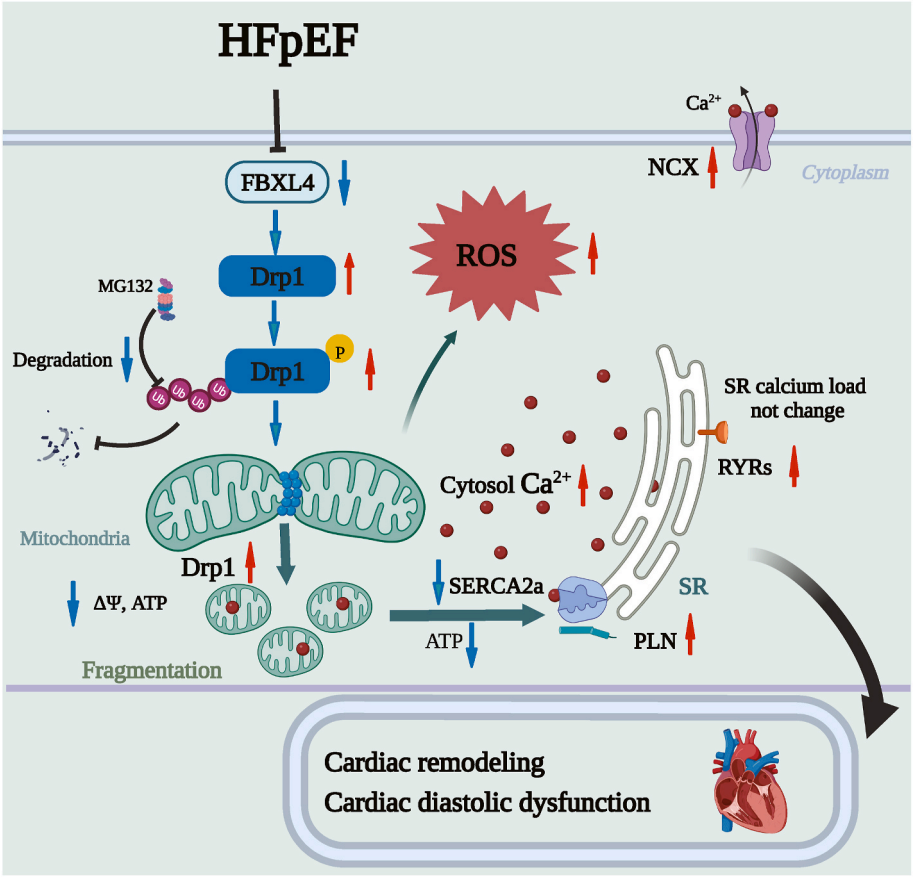

Fig. 9. Schematic diagram exhibiting possible involvement of FBXL4 in HFpEF-associated cardiomyopathy through FBXL4-evoked Drp1 degradation in a proteasomal-dependent manner. HFpEF downregulates FBXL4 level, resulting hyperactivation of Drp1 and subsequent mitochondrial injury. Elevated FBXL4 level rescues against HFpEF-induced cardiac remodeling, diastolic dysfunction, and mitochondrial injury (mitochondrial fragmentation, collapsed membrane potential and intracellular Ca^{2+} overload due to defective SERCA2a function) through reverting hyperactivation of Drp1-mediated mitochondrial fission.

serve as possible targets for HFpEF therapeutics.

Funding

This work was supported by the Shanghai Municipal Key Clinical Specialty (shslczdzk01701), Natural Science Foundation of China (82130011, RFIS82250710173, 81900233, 92249301), and Shanghai Xuhui District Scientific Research Project (202104, 202105).

CRediT authorship contribution statement

Miyesaier Abudureyimu: Methodology, Investigation, Formal analysis, Data curation, Conceptualization. **Xuanming Luo:** Formal analysis, Data curation, Conceptualization. **Lingling Jiang:** Investigation, Formal analysis. **Xuejuan Jin:** Formal analysis, Data curation. **Cuizhen Pan:** Formal analysis, Data curation. **Wei Yu:** Investigation, Formal analysis. **Junbo Ge:** Supervision. **Yingmei Zhang:** Supervision, Funding acquisition, Conceptualization. **Jun Ren:** Supervision, Funding acquisition, Conceptualization.

Declaration of competing interest

None of the authors has any conflict of interest to declare.

Data availability

Data will be made available on request.

Acknowledgement

We would like to thank Dr Yu Kong and Xu Wang (Electron Microscopy Facilities of Center for Excellence in Brain Science and Technology, Chinese Academy of Science) for assistance with EM sample preparation and EM image analysis. We are also grateful to Wuhan Metware Biotechnology Co. Ltd (Wuhan, China) for technical assistance.

Appendix A. Supplementary data

Supplementary data to this article can be found online at https://doi.org/10.1016/j.redox.2024.103081.

References

[1] M. Abudureyimu, et al., Heart failure with preserved ejection fraction (HFpEF) in type 2 diabetes mellitus: from pathophysiology to therapeutics, J. Mol. Cell Biol. 14 (2022) mjac028, https://doi.org/10.1093/jmcb/mjac028.
[2] K.S. Shah, et al., Heart failure with preserved, borderline, and reduced ejection fraction: 5-year outcomes, J. Am. Coll. Cardiol. 70 (2017) 2476–2486, https://doi.org/10.1016/j.jacc.2017.08.074.
[3] A. Del Campo, G. Perez, P.F. Castro, V. Parra, H.E. Verdejo, Mitochondrial function, dynamics and quality control in the pathophysiology of HFpEF, Biochim. Biophys. Acta, Mol. Basis Dis. 1867 (2021) 166208, https://doi.org/10.1016/j.bbadis.2021.166208.
[4] M. Abudureyimu, et al., Berberine alleviates myocardial diastolic dysfunction by modulating Drp1-mediated mitochondrial fission and Ca(2+) homeostasis in a murine model of HFpEF, Front. Med. (2023), https://doi.org/10.1007/s11684-023-0983-0.
[5] S. Sanders-van Wijk, et al., Proteomic evaluation of the comorbidity-inflammation paradigm in heart failure with preserved ejection fraction: results from the PROMIS-HFpEF study, Circulation 142 (2020) 2029–2044, https://doi.org/10.1161/CIRCULATIONAHA.120.045810.
[6] N. Savji, et al., The association of obesity and cardiometabolic traits with incident HFpEF and HFrEF, JACC Heart Fail 6 (2018) 701–709, https://doi.org/10.1016/j.jchf.2018.05.018.
[7] A.A. Kumar, D.P. Kelly, J.A. Chirinos, Mitochondrial dysfunction in heart failure with preserved ejection fraction, Circulation 139 (2019) 1435–1450, https://doi.org/10.1161/CIRCULATIONAHA.118.036259.
[8] A. Ajoolabady, M. Chiong, S. Lavandero, D.J. Klionsky, J. Ren, Mitophagy in cardiovascular diseases: molecular mechanisms, pathogenesis, and treatment, Trends Mol. Med. 28 (2022) 836–849, https://doi.org/10.1016/j.molmed.2022.06.007.
[9] C. Sotomayor-Flores, et al., Angiotensin-(1-9) prevents cardiomyocyte hypertrophy by controlling mitochondrial dynamics via miR-129-3p/PKIA pathway, Cell Death Differ. 27 (2020) 2586–2604, https://doi.org/10.1038/s41418-020-0522-3.
[10] H. Xu, et al., Syntaxin17 contributes to obesity cardiomyopathy through promoting mitochondrial Ca(2+) overload in a Parkin-MCUb-dependent manner, Metabolism 143 (2023) 155551, https://doi.org/10.1016/j.metabol.2023.155551.
[11] J. Ren, L. Pulakat, A. Whaley-Connell, J.R. Sowers, Mitochondrial biogenesis in the metabolic syndrome and cardiovascular disease, J. Mol. Med. (Berl.) 88 (2010) 993–1001, https://doi.org/10.1007/s00109-010-0663-9.
[12] V.S. Hahn, et al., Myocardial gene expression signatures in human heart failure with preserved ejection fraction, Circulation 143 (2021) 120–134, https://doi.org/10.1161/CIRCULATIONAHA.120.050498.
[13] L. Wang, et al., DNA-dependent protein kinase catalytic subunit (DNA-PKcs) drives angiotensin II-induced vascular remodeling through regulating mitochondrial fragmentation, Redox Biol. 67 (2023) 102893, https://doi.org/10.1016/j.redox.2023.102893.
[14] H. Xu, et al., Syntaxin 17 protects against heart failure through recruitment of CDK1 to promote DRP1-dependent mitophagy, JACC Basic Transl Sci 8 (2023) 1215–1239, https://doi.org/10.1016/j.jacbts.2023.04.006.
[15] M. Valera-Alberni, et al., Crosstalk between Drp1 phosphorylation sites during mitochondrial remodeling and their impact on metabolic adaptation, Cell Rep. 36 (2021) 109565, https://doi.org/10.1016/j.celrep.2021.109565.
[16] M. Roy, K. Itoh, M. Iijima, H. Sesaki, Parkin suppresses Drp1-independent mitochondrial division, Biochem. Biophys. Res. Commun. 475 (2016) 283–288, https://doi.org/10.1016/j.bbrc.2016.05.038.
[17] J. Ren, et al., FUNDC1 interacts with FBXL2 to govern mitochondrial integrity and cardiac function through an IP3R3-dependent manner in obesity, Sci. Adv. 6 (2020) eabc8561, https://doi.org/10.1126/sciadv.abc8561.
[18] C. Bai, et al., SKP1 connects cell cycle regulators to the ubiquitin proteolysis machinery through a novel motif, the F-box, Cell 86 (1996) 263–274, https://doi.org/10.1016/s0092-8674(00)80098-7.
[19] D. Alsina, et al., FBXL4 deficiency increases mitochondrial removal by autophagy, EMBO Mol. Med. 12 (2020) e11659, https://doi.org/10.15252/emmm.201911659.
[20] R. Sabouny, et al., Characterization of the C584R variant in the mtDNA depletion syndrome gene FBXL4, reveals a novel role for FBXL4 as a regulator of mitochondrial fusion, Biochim. Biophys. Acta, Mol. Basis Dis. 1865 (2019) 165536, https://doi.org/10.1016/j.bbadis.2019.165536.
[21] G.G. Schiattarella, et al., Nitrosative stress drives heart failure with preserved ejection fraction, Nature 568 (2019) 351–356, https://doi.org/10.1038/s41586-019-1100-z.
[22] M. Sun, et al., NDP52 protects against myocardial infarction-provoked cardiac anomalies through promoting autophagosome-lysosome fusion via recruiting TBK1 and RAB7, Antioxidants Redox Signal. 36 (2022) 1119–1135, https://doi.org/10.1089/ars.2020.8253.
[23] A. Shirakabe, et al., Drp1-Dependent mitochondrial autophagy plays a protective role against pressure overload-induced mitochondrial dysfunction and heart failure, Circulation 133 (2016) 1249–1263, https://doi.org/10.1161/CIRCULATIONAHA.115.020502.
[24] M. Galderisi, et al., Standardization of adult transthoracic echocardiography reporting in agreement with recent chamber quantification, diastolic function, and heart valve disease recommendations: an expert consensus document of the European Association of Cardiovascular Imaging, Eur Heart J Cardiovasc Imaging 18 (2017) 1301–1310, https://doi.org/10.1093/ehjci/jex244.
[25] G.P. Stefani, et al., Effects of aerobic and resistance exercise training associated with carnosine precursor supplementation on maximal strength and VO(2max) in rats with heart failure, Life Sci. 282 (2021) 119816, https://doi.org/10.1016/j.lfs.2021.119816.
[26] Z. Huskova, et al., Intrarenal alterations of the angiotensin-converting enzyme type 2/angiotensin 1-7 complex of the renin-angiotensin system do not alter the course of malignant hypertension in Cyp1a1-Ren-2 transgenic rats, Clin. Exp. Pharmacol. Physiol. 43 (2016) 438–449, https://doi.org/10.1111/1440-1681.12553.
[27] A. Besse, et al., AAV9-Mediated expression of SMN restricted to neurons does not rescue the spinal muscular atrophy phenotype in mice, Mol. Ther. 28 (2020) 1887–1901, https://doi.org/10.1016/j.ymthe.2020.05.011.
[28] Q.Q. Chen, et al., Neuraminidase 1 is a driver of experimental cardiac hypertrophy, Eur. Heart J. 42 (2021) 3770–3782, https://doi.org/10.1093/eurheartj/ehab347.
[29] J. Ren, L.E. Wold, Measurement of cardiac mechanical function in isolated ventricular myocytes from rats and mice by computerized video-based imaging, Biol. Proced. Online 3 (2001) 43–53, https://doi.org/10.1251/bpo22.
[30] H. Xu, et al., TAX1BP1 protects against myocardial infarction-associated cardiac anomalies through inhibition of inflammasomes in a RNF34/MAVS/NLRP3-dependent manner, Sci. Bull. 66 (2021) 1669–1683, https://doi.org/10.1016/j.scib.2021.01.030.
[31] A.F. Ceylan, et al., Cardiomyocyte-specific knockout of endothelin receptor a attenuates obesity cardiomyopathy, Biochim. Biophys. Acta, Mol. Basis Dis. 1864 (2018) 3339–3352, https://doi.org/10.1016/j.bbadis.2018.07.020.
[32] H. Xu, et al., Luteolin attenuates doxorubicin-induced cardiotoxicity through promoting mitochondrial autophagy, Front. Physiol. 11 (2020) 113, https://doi.org/10.3389/fphys.2020.00113.
[33] W. Yu, W. Zha, Ren, J. Exendin-4 and liraglutide attenuate glucose toxicity-induced cardiac injury through mTOR/ULK1-dependent autophagy, Oxid. Med. Cell. Longev. (2018) 5396806, https://doi.org/10.1155/2018/5396806, 2018.
[34] S. Sun, et al., TBC1D15-Drp1 interaction-mediated mitochondrial homeostasis confers cardioprotection against myocardial ischemia/reperfusion injury, Metabolism 134 (2022) 155239, https://doi.org/10.1016/j.metabol.2022.155239.

[35] W.J.H. Paulus, (2)FPEF score: at last, a properly validated diagnostic algorithm for heart failure with preserved ejection fraction, Circulation 138 (2018) 871–873, https://doi.org/10.1161/CIRCULATIONAHA.118.035711.
[36] X. Cui, et al., Prevalence and correlates of left ventricular diastolic dysfunction and heart failure with preserved ejection fraction in elderly community residents, Int. J. Cardiol. 227 (2017) 820–825, https://doi.org/10.1016/j.ijcard.2016.10.041.
[37] C. Bi, et al., A proteomics- and metabolomics-based study revealed that disorder of palmitic acid metabolism by aconitine induces cardiac injury, Chem. Res. Toxicol. 33 (2020) 3031–3040, https://doi.org/10.1021/acs.chemrestox.0c00372.
[38] L. Yang, et al., Cardiac-specific overexpression of metallothionein attenuates L-NAME-induced myocardial contractile anomalies and apoptosis, J. Cell Mol. Med. 23 (2019) 4640–4652, https://doi.org/10.1111/jcmm.14375.
[39] Q. Wang, et al., Maternal obesity impairs fetal cardiomyocyte contractile function in sheep, FASEB J 33 (2019) 2587–2598, https://doi.org/10.1096/fj.201800988R.
[40] Z. Pei, et al., FUNDC1 insufficiency sensitizes high fat diet intake-induced cardiac remodeling and contractile anomaly through ACSL4-mediated ferroptosis, Metabolism 122 (2021) 154840, https://doi.org/10.1016/j.metabol.2021.154840.
[41] J. Ren, A.J. Davidoff, R.A. Brown, Acetaldehyde depresses shortening and intracellular Ca2+ transients in adult rat ventricular myocytes, Cell. Mol. Biol. (Noisy-Le-Grand) 43 (1997) 825–834.
[42] Z. Chen, et al., Mitochondrial E3 ligase MARCH5 regulates FUNDC1 to fine-tune hypoxic mitophagy, EMBO Rep. 18 (2017) 495–509, https://doi.org/10.15252/embr.201643309.
[43] H. Otera, et al., Mff is an essential factor for mitochondrial recruitment of Drp1 during mitochondrial fission in mammalian cells, J. Cell Biol. 191 (2010) 1141–1158, https://doi.org/10.1083/jcb.201007152.
[44] L. Schwarzmann, R.U. Pliquett, A. Simm, B. Bartling, Sex-related differences in human plasma NAD+/NADH levels depend on age, Biosci. Rep. 41 (2021), https://doi.org/10.1042/BSR20200340.
[45] E.M. Palmieri, et al., Nitric oxide orchestrates metabolic rewiring in M1 macrophages by targeting aconitase 2 and pyruvate dehydrogenase, Nat. Commun. 11 (2020) 698, https://doi.org/10.1038/s41467-020-14433-7.
[46] C. Quan, M. Li, Q. Du, Q. Chen, H. Wang, D. Campbell, L. Fang, B. Xue, C. MacKintosh, X. Gao, K. Ouyang, H.Y. Wang, S. Chen, SPEG Controls Calcium Reuptake Into the Sarcoplasmic Reticulum Through Regulating SERCA2a by Its Second Kinase-Domain, Circ Res. 124 (5) (2019 Mar) 712–726, https://doi.org/10.1161/CIRCRESAHA.118.313916. Erratum in: Circ Res. 2019 Dec 6;125(12): e113. PMID: 30566039.
[47] A.H. Chaanine, et al., Mitochondrial morphology, dynamics, and function in human pressure overload or ischemic heart disease with preserved or reduced ejection fraction, Circ Heart Fail 12 (2019) e005131, https://doi.org/10.1161/CIRCHEARTFAILURE.118.005131.
[48] S.J. Shah, et al., Prevalence and correlates of coronary microvascular dysfunction in heart failure with preserved ejection fraction: PROMIS-HFpEF, Eur. Heart J. 39 (2018) 3439–3450, https://doi.org/10.1093/eurheartj/ehy531.
[49] M. Abudureyimu, et al., The impact of hypertension on left ventricular diastolic dysfunction and arterial stiffness in the elderly: a cross-sectional study, Cardiol. Plus. 5 (2020) 186–193.
[50] A. Ajoolabady, J.H. Tuomilehto, G.Y. Lip, D.J. Klionsky, J. Ren, Deciphering the role of autophagy in heart failure, Cardiol. 6 (2021) 92–101.
[51] X. Gai, et al., Mutations in FBXL4, encoding a mitochondrial protein, cause early-onset mitochondrial encephalomyopathy, Am. J. Hum. Genet. 93 (2013) 482–495, https://doi.org/10.1016/j.ajhg.2013.07.016.
[52] P.E. Bonnen, et al., Mutations in FBXL4 cause mitochondrial encephalopathy and a disorder of mitochondrial DNA maintenance, Am. J. Hum. Genet. 93 (2013) 471–481, https://doi.org/10.1016/j.ajhg.2013.07.017.
[53] S. Wang, et al., Novel homozygous mutation in the FBXL4 gene is associated with mitochondria DNA depletion syndrome-13, J. Neurol. Sci. 416 (2020) 116948, https://doi.org/10.1016/j.jns.2020.116948.
[54] G. Antoun, et al., Detailed biochemical and bioenergetic characterization of FBXL4-related encephalomyopathic mitochondrial DNA depletion, JIMD Rep 27 (2016) 1–9, https://doi.org/10.1007/8904_2015_491.
[55] M. Tong, D. Zablocki, J. Sadoshima, The role of Drp1 in mitophagy and cell death in the heart, J. Mol. Cell. Cardiol. 142 (2020) 138–145, https://doi.org/10.1016/j.yjmcc.2020.04.015.
[56] Y. Ikeda, et al., Endogenous Drp1 mediates mitochondrial autophagy and protects the heart against energy stress, Circ. Res. 116 (2015) 264–278, https://doi.org/10.1161/CIRCRESAHA.116.303356.
[57] B. Westermann, Mitochondrial fusion and fission in cell life and death, Nat. Rev. Mol. Cell Biol. 11 (2010) 872–884, https://doi.org/10.1038/nrm3013.
[58] Z. Zhang, L. Liu, S. Wu, D. Xing, Drp1, Mff, Fis1, and MiD51 are coordinated to mediate mitochondrial fission during UV irradiation-induced apoptosis, in: FASEB Journal : Official Publication of the Federation of American Societies for Experimental Biology, 30, 2016, pp. 466–476, https://doi.org/10.1096/fj.15-274258.
[59] M. Zhang, A. Perino, A. Ghigo, E. Hirsch, A.M. Shah, NADPH oxidases in heart failure: poachers or gamekeepers? Antioxidants Redox Signal. 18 (2013) 1024–1041, https://doi.org/10.1089/ars.2012.4550.
[60] D. Terentyev, et al., Redox modification of ryanodine receptors contributes to sarcoplasmic reticulum Ca2+ leak in chronic heart failure, Circ. Res. 103 (2008) 1466–1472, https://doi.org/10.1161/CIRCRESAHA.108.184457.
[61] P. van der Meer, H.K. Gaggin, G.W. Dec, ACC/AHA versus ESC guidelines on heart failure: JACC guideline comparison, J. Am. Coll. Cardiol. 73 (2019) 2756–2768, https://doi.org/10.1016/j.jacc.2019.03.478.
[62] J. Ren, N.N. Wu, S. Wang, J.R. Sowers, Y. Zhang, Obesity cardiomyopathy: evidence, mechanisms, and therapeutic implications, Physiol. Rev. 101 (2021) 1745–1807, https://doi.org/10.1152/physrev.00030.2020.
[63] C. Cenciarelli, et al., Identification of a family of human F-box proteins, Curr. Biol. 9 (1999) 1177–1179.
[64] U. Schmidt, et al., Contribution of abnormal sarcoplasmic reticulum ATPase activity to systolic and diastolic dysfunction in human heart failure, J. Mol. Cell. Cardiol. 30 (1998) 1929–1937, https://doi.org/10.1006/jmcc.1998.0748.
[65] L.E. Wold, et al., Impaired SERCA function contributes to cardiomyocyte dysfunction in insulin resistant rats, J. Mol. Cell. Cardiol. 39 (2005) 297–307, https://doi.org/10.1016/j.yjmcc.2005.03.014.
[66] E. Torre, et al., SERCA2a stimulation by istaroxime improves intracellular Ca2+ handling and diastolic dysfunction in a model of diabetic cardiomyopathy, Cardiovasc. Res. 118 (2022) 1020–1032, https://doi.org/10.1093/cvr/cvab123.
[67] S. Zhu, et al., Loss of myocardial retinoic acid receptor alpha induces diastolic dysfunction by promoting intracellular oxidative stress and calcium mishandling in adult mice, J. Mol. Cell. Cardiol. 99 (2016) 100–112, https://doi.org/10.1016/j.yjmcc.2016.08.009.
[68] E.E. van Riet, et al., Epidemiology of heart failure: the prevalence of heart failure and ventricular dysfunction in older adults over time. A systematic review, Eur. J. Heart Fail. 18 (2016) 242–252, https://doi.org/10.1002/ejhf.483.
[69] G.F. Mureddu, et al., Prevalence of preclinical and clinical heart failure in the elderly. A population-based study in Central Italy, Eur. J. Heart Fail. 14 (2012) 718–729, https://doi.org/10.1093/eurjhf/hfs052.
[70] J. Tromp, et al., Age-related characteristics and outcomes of patients with heart failure with preserved ejection fraction, J. Am. Coll. Cardiol. 74 (2019) 601–612, https://doi.org/10.1016/j.jacc.2019.05.052.
[71] A. Ajoolabady, H. Aslkhodapasandhokmabad, A. Aghanejad, Y. Zhang, J. Ren, Mitophagy receptors and mediators: therapeutic targets in the management of cardiovascular ageing, Ageing Res. Rev. 62 (2020) 101129, https://doi.org/10.1016/j.arr.2020.101129.